A RE-EVALUATION OF THE VOLCANIC HISTORY AND MINERAL POTENTIAL OF THE CENTRAL EAST TINTIC MOUNTAINS, UTAH

Jeffrey D. Keith, R. David Dallmeyer, and Choon-Sik Kim
Department of Geology, University of Georgia

and
Bart J. Kowallis
Department of Geology, Brigham Young University

UTAH GEOLOGICAL AND MINERAL SURVEY
a division of
UTAH DEPARTMENT OF NATURAL RESOURCES
OPEN-FILE REPORT 166 **1989**

THE PUBLICATION OF THIS PAPER
IS MADE POSSIBLE WITH MINERAL LEASE FUNDS

A RE-EVALUATION OF THE VOLCANIC HISTORY AND MINERAL POTENTIAL OF THE CENTRAL EAST TINTIC MOUNTAINS, UTAH

Submitted to the UGMS on:

September 20, 1989

in fulfillment of contract # 88 3548

Jeffrey D. Keith
and
R. David Dallmeyer
and
Choon-Sik Kim

Department of Geology
The University of Georgia
Athens, Georgia 30602
(404)-542-2652

Bart J. Kowallis

Department of Geology
Brigham Young University
Provo, Utah 84602
(801)-378-2467

TABLE OF CONTENTS

ABSTRACT

This report documents several new findings concerning the geology and mineral potential of the central East Tintic Mountains, Utah. For example, fission-track ages and $^{40}Ar/^{39}Ar$ ages which we report suggest that some of the volcanism and alteration in this area is as old as 37.4 to 35.3 Ma. This early episode of volcanism was contemporaneous with lacustrine deposition; the overlying volcanic rocks and cross-cutting intrusions range in age from about 34.5 to 33.6 Ma. This implies that a large caldera related to the eruption of the younger Packard Quartz Latite and Fernow Quartz Latite is not present in this area. However, our data suggest that a smaller caldera related to the eruption of the tuff member of the Copperopolis Latite may be present. We note that many monzonite dikes and intrusions in this area are hornblende bearing and are correlative in modal and chemical composition with the productive Silver City Stock rather than the barren Sunrise Peak Stock. The large areas of hydrothermal alteration which surround these intrusions exhibit many similarities to the well-studied alteration halos in the East Tintic District. The age, composition, and field relationships of the post-lacustrine volcanic rocks suggest that they may represent, in part, the extrusive equivalents of the monzonite dikes and Silver City Stock. Our work suggests that the Silver City Stock and related intrusions may be part of one of the youngest (33.6 $\pm$ 0.2 Ma) igneous events in the central East Tintic Mountains, but not as young as previously suggested (ca. 31.5 Ma).

In addition, our recent work has documented the existence of unusually large (and abundant) magmatic sulfides in lava vitrophyres and vent-facies biotite latite dikes, which are the surface expressions of the Silver City Quartz Monzonite intrusions in this area. In addition, preliminary analytical data suggest that the sulfides host most (~75%) of the Ag present in the

latites. The East Tintic Mountains are potentially the first locality, worldwide, where Ag in mesothermal veins can be demonstrated to be derived from degassed Ag-bearing magmatic sulfides. Consequently, the central East Tintic Mountains are a favorable area for exploration for Ag (Pb-Zn-Cu-Au) ore bodies because: 1) productive monzonite intrusions are present, and 2) Paleozoic rocks favorable for ore deposition may be present beneath relatively thin volcanic cover because the area is not entirely enclosed within a caldera.

INTRODUCTION

Morris and Lovering (1979) suggest that the ages of all the volcanic and intrusive units in the East Tintic Mountains cluster into two groups of about 32-33 and 18 m.y. old. However, they do report some older ages (35-39 m.y.), which they consider to be anomalous. They suggest that most volcanic units in the East Tintic District were deposited in an area of moderate topographic relief, analogous to the East Tintic Mountains today. They hypothesize that the initial ash-flow eruption deposited the Packard Quartz Latite and Fernow Quartz Latite and created a caldera 14 km in diameter in the central portion of the East Tintic Mountains (Figure 1; Morris, 1975). Subsequently, latite flows, ash flows, and hypabyssal intrusions of the Tintic Mountain Volcanic Group filled and overflowed the caldera. These two events were followed closely in time by a final episode of Oligocene latitic volcanism and consanguineous intrusions (Silver City stock and correlative dikes; Figure 1) which appears to be genetically related to all of the mineralization in these districts (Morris and Lovering, 1979).

This report documents the occurrence of previously unrecognized Eocene-Oligocene (ca. 37-35 m.y.) volcanic and intrusive lithologies and lacustrine sediments (up to 50 m thick). These events were followed by volcanic and intrusive activity which ranged in age from roughly 34.5 to 33.6 Ma. The

study area also includes an area of strong hydrothermal alteration and diking in the central East Tintic Mountains (Figure 1). To our knowledge, very little geochemical prospecting of this area has been done (by others or as part of this study). The alteration assemblages present in this area (silicification and abundant pyrite in carbonate-bearing sediments) suggest several analogies to alteration in the East Tintic District.

The lacustrine sediments clearly affected the character of the widespread hydrothermal alteration in Government Canyon. Alteration products in the volcanic rocks overlying the sediments are indicative of more neutral pH conditions compared to the argillic alteration below the sediments. In addition, larger amounts of pyrite and jasperoid are generally found in the sediments than in subjacent volcanic rocks. These and other facets of the alteration assemblages present in Government Canyon are very analogous (and probably of equivalent age) to the well-studied alteration halos in volcanic rocks in the East Tintic district (Lovering, 1949). At the surface, acidic hydrothermal solutions in Government Canyon were mostly neutralized during passage through Oligocene sediments rather than along veins in Paleozoic rocks. However, several lines of reasoning suggest that the volcanic cover becomes thinner to the East and North in this portion of the East Tintic Mountains; consequently, exploration in areas of favorable hydrothermal alteration may be feasible.

The Tintic and East Tintic Districts have long been recognized as clearly exemplifying the spatial relationships between sulfide-rich alteration, Ag (-Au) mineralization, and productive intrusions (Lindgren and Loughlin, 1919; Lovering, 1949; Morris and Lovering, 1979). However, whether the precious metals are derived from the intrusions or merely leached from the country rock by hydrothermal circulation has not been convincingly demonstrated for this

district or any epithermal-mesothermal vein deposit. Our recent work (during the last year) has documented the existence of unusually large magmatic sulfides in vent-facies dikes (and lava vitrophyres) which are the surface expressions of the productive intrusions in the East Tintic Mountains. In addition, preliminary analytical data suggest that the sulfides may host most (~75%) of the Ag present in the latites. To our knowledge, such a close correspondence between intrusions with unusually abundant magmatic sulfides and hydrothermal mineralization has not been previously demonstrated. However, Whitney and Stormer (1983) speculated that a general relationship between degassing calc-alkaline pyrrhotite-bearing magmas and hydrothermal ore deposits was possible. The East Tintic Mountains are potentially the first locality, worldwide, where Ag in mesothermal veins can be demonstrated to be derived from degassed Ag-bearing magmatic sulfides.

METHODS

X-Ray Fluorescence and Electron Microprobe Techniques

Approximately 150 samples of extrusive and intrusive units were collected and examined in thin section or polished section. Whole-rock sulfur analyses were done by X-ray fluorescence spectrometry using pressed powder pellets with G-2, GSP-1, and W-1 as standards. Whole-rock major elements were analysed using a fused disk procedure (Norish and Hutton, 1969) with the USGS standard AGV-1 used as an internal standard. Microprobe analyses were done at the University of South Carolina using a Cameca SX-50 electron microprobe. Descriptions and locations of samples used for analysis are given in Appendix 1.

$^{40}Ar/^{39}Ar$ Analytical Techniques

Optically pure (> 99%) mineral concentrates were wrapped in aluminum-foil packets, encapsulated in sealed quartz vials and irradiated in either the U.S.

Geological Survey TRIGA reactor (samples HS-UTH-86-2, TJ-84-88, TJ-112-88, TJ-77-88) or the H-5 position of the Ford Reactor at the University of Michigan (samples TJ-8-87 and KS-2A-87). Variations in the flux of neutrons along the length of the irradiation assembly were monitored with several mineral standards, including MMhb-1 (Alexander et al. 1978). The samples were incrementally heated until fusion in a double-vacuum, resistance heated furnace. Temperatures were monitored with a direct-contact thermocouple and are controlled to $\pm$ 1°C between increments and are accurate to $\pm$ 5°C. Measured isotopic ratios were corrected for total system blanks and the effects of mass discrimination. Interfering isotopes produced during irradiation were corrected using factors reported by Dalrymple et al. (1981) for the TRIGA reactor or Harrison and Fitzgerald (1986) for the Ford Reactor. Apparent $^{40}Ar/^{39}Ar$ ages were calculated from the corrected isotopic ratios using the decay constants and isotopic abundance ratios listed by Steiger and Jager (1977).

Two categories of uncertainties are encountered in $^{40}Ar/^{39}Ar$ incremental-release dating. One group involves intralaboratory uncertainties related to measurement of the isotopic ratios used in the age equation. The other group considers interlaboratory uncertainties in other parameters used in the age equation (monitor age, J-value determination, etc.), and are the same for each gas increment evolved from a particular sample. Therefore, to evaluate the significance of incremental age variations within a single sample, only intralaboratory uncertainties should be considered. These are reported here and have been calculated by statistical propagation of uncertainties associated with measurement of each isotopic ratio (at two standard deviations of the mean) through the age equation. Interlaboratory uncertainties are approximately 1.25-1.50% of the quoted age. Total-gas ages have been computed for each sample by appropriate weighting of the age and percent ^{39}Ar released within

each temperature increment. A "plateau" is herein considered to be defined if the ages recorded by two or more contiguous gas fractions, each representing >4% of the total ^{39}Ar evolved and characterized by generally similar apparent K/Ca ratios (and together constituting >50% of the total quantity of ^{39}Ar evolved) are mutually similar within a ± 1% intralaboratory uncertainty. Analyses of the MMhb-1 monitor indicate that apparent K/Ca ratios may be calculated through the relationship 0.518 (± 0.005) x $^{39}Ar/^{37}Ar$ corrected (TRIGA reactor) or 0.505 (± 0.003) x $^{39}Ar/^{37}Ar$ corrected (Ford Reactor).

Plateau portions of the analyses have been plotted on $^{36}Ar/^{40}Ar$ vs. $^{39}Ar/^{40}Ar$ isotope correlation diagrams (Roddick et al. 1980, Radicati de Brozolo et al. 1981). Regression techniques followed the methods of York (1969). A mean square of the weighted deviates (MSWD) is the statistical parameter which has been used to evaluate isotopic correlations. Roddick (1978) suggests that an MSWD > c. 2.5 indicates scatter about a correlation line greater than that which can be explained only by experimental errors.

RESULTS

$^{40}Ar/^{39}Ar$ Results

Four biotite, one sanidine, and one muscovite concentrate have been prepared from samples collected within volcanic units exposed in the East Titnic Mountains, Utah. Location coordinates and detailed petrographic descriptions of the analyzed samples are provided in Appendix 1. The $^{40}Ar/^{39}Ar$ analytical data are listed in Table 8, and are presented as incremental age spectra in Figure 7. Results of $^{36}Ar/^{40}Ar$ vs. $^{39}Ar/^{40}Ar$ isotope correlations of the analysis are listed in Table 9.

The four biotite concentrates display internally discordant $^{40}Ar/^{39}Ar$ age

spectra corresponding to total-gas ages ranging between 37.9 ± 0.2 Ma (TJ-8-87) and 34.0 ± 0.4 Ma (HS-UTH-86-2). Apparent K-Ca spectra are internally variable. The low-temperature increments are generally characterized by systematically increasing apparent K/Ca ratios and systematically decreasing apparent ages. Intermediate-temperature gas fractions are characterized by very large and only slightly fluctuating apparent K/Ca ratios. These increments generally record mutually similar apparent ages within each analysis, and define plateau ages of 37.4 ± 0.3 Ma (TJ-8-87), 35.3 ± 0.1 Ma (TJ-112-88), 34.5 ± 0.2 Ma (TJ-84-88) and 33.6 ± 0.2 Ma (HS-UTH-86-2). Higher temperature portions of each analysis generally display systematically decreasing apparent K/Ca ratios and record somewhat variable apparent ages. The plateau analytical data yield well-defined $^{36}Ar/^{40}Ar$ vs. $^{39}Ar/^{40}Ar$ isotope correlations (MSWD = 0.14-1.84: Table 2) with inverse ordinate intercepts similar to the $^{40}Ar/^{36}Ar$ ratio within the present-day atmosphere (295.5). This indicates a lack of significant extraneous ("excess") argon contamination within constituent biotite grains. Using the inverse abscissa intercepts in the age equation yields plateau isotope correlation ages similar to those calculated for each sample directly from the analytical data.

The muscovite concentrate from sample KS-2A-87 displays internally discordant apparent age and K/Ca spectra with a total-gas age of 36.5 ± 0.6 Ma. The 450-660°C temperature fractions are characterized by large and generally similar apparent K/Ca ratios. These increments define a plateau age of 36.7 ± 0.5 Ma. The four high-temperature gas fractions display markedly fluctuating apparent K/Ca ratios and record somewhat variable apparent ages. The plateau data yields an isotope correlation (MSWD = 0.19) with an inverse ordinate intercept of 346.3 ± 31.3. Using the inverse abscissa intercept in the age

equation results in a plateau isotope correlation age of 36.6 ± 0.2 Ma.

The sanidine muscovite concentrate from sample TJ-77-98 also displays internally discordant apparent age and apparent K/Ca spectra with a total-gas age of 34.3 ± 0.2 Ma. Apparent K/Ca ratios systematically increase throughout the 700-1020°C portions of the analysis. However, the 800-1020°C increments record mutually similar apparent ages which define a plateau age of 34.1 ± 0.1 Ma. The two high-temperature increments record lower apparent K/Ca ratios and define younger apparent ages. The plateau analytical data result in an isotope correlation (MSWD = 0.43) with an inverse ordinate intercept of 360.3 ± 42.6. Using the inverse abscissa intercept in the age equation yields a plateau isotope correlation age of 34.0 ± 0.1 Ma.

Interpretation

During the biotite analyses, intrasample fluctuations in apparent K/Ca ratios suggest experimental evolution of argon occurred from several compositionally distinct, and variably retentive phases. These could be represented by: 1) very minor, optically undetectable mineralogical contaminants in the biotite concentrates; 2) petrographically unresolvable exsolution or compositional zonation within constituent biotite grains; and/or, 3) intracrystalline inclusions. Gas increments evolved during most intermediate-temperature increments are characterized by mutually similar apparent K/Ca ratios, indicating experimental evolution of gas from compositionally uniform populations of intracrystalline sites. Apparent ages recorded by intermediate-temperature increments evolved from each of the biotite concentrates are similar isotope correlations ages indicating a lack of significant extraneous argon contamination. Because of these relationships the biotite plateau ages are considered geologically meaningful.

Low- and intermediate-temperature portions of the muscovite analysis are characterized by generally uniform apparent K/Ca ratios indicating experimental evolution of gas from a compositionally uniform population of intracrystalline sites. The higher temperature gas fractions display markedly fluctuating apparent K/Ca ratios which likely reflect experimental evolution of gas from minor, optically undetectable mineralogical contaminates in the muscovite concentrate. The low- and intermediate temperature increments yield a well-defined plateau age which is similar to that resulting from isotope correlation of the plateau data. This suggests the muscovite plateau age is geologically meaningful.

Consistent intrasample variations in apparent K/Ca ratios in low- and intermediate-temperature portions of the sanidine analysis suggests that compositionally variable intracrystalline sites contributed gas during the experiment. However, most of these increments record similar apparent ages which define a plateau. These data yield a similar isotope correlation age indicating the sanidine plateau age may be considered geologically reliable.

Revised Volcanic and Intrusive Sequence

Our mapping in the central East Tintic Mountains indicates the occurrence of several significant sedimentary and volcanic units not recognized by Morris and Lovering (1979; Morris, 1975). For example, two lacustrine sedimentary horizons are intercalated with ash-flow tuff and flow/agglomerate members of the Copperopolis Latite. The lower sedimentary horizon (0-50 m) overlies an ash-flow tuff member (the upper portion of which is moderately reworked) and consists dominantly of fissile shale with lesser amounts of mudstone and volcaniclastic sandstone (Figure 2). The coarser-grained horizons in this unit generally contain the greater amount of carbonate cement. Small (~1 cm),

primary ovoidal structures in the shaley horizons probably represent calcareous gastropod shells which have been replaced by pyrite and subsequently converted to limonite (Figure 2).

The upper lacustrine horizon is separated from the lower by a previously unmapped flow and agglomerate member of the Copperopolis Latite. The agglomerate often contains deformed clasts of shale or mud (between large blocks) that were apparently ripped up from the lake bottom during deposition. The flows which occupy this stratigraphic position near Sunrise Peak apear to have vented from Sunrise Peak Stock (as first suggested by Lindgren and Laughlin, 1919) and dikes of similar composition to the north. Consequently, we informally refer to this unit as the flows and agglomerates of Sunrise Peak (Plate 1). The upper lacustrine horizon (0-20 m) overlies a few meters of finer, reworked volcanic material and consists of alternating beds of organic-rich shale (abundant plant remains) and limestone (0-3 m; Figure 3).

Fission-track dating of apatites extracted from the volcaniclastic material in each of the two lacustrine horizons suggests an approximate age of about 36-37 m.y. (Table 1) for this episode of volcanism and sedimentation. In addition, $^{40}Ar/^{39}Ar$ ages for biotite from a biotite latite vitrophyre (sample # TJ-8; 37.4 $\pm$ 0.3 Ma) and sericite from the lower lacustrine horizon (sample # KS-2A; 36.7 $\pm$ 0.5 Ma; Figure 7) suggest approximately the same ages for some of the volcanic and intrusive units beneath the lacustrine horizons. Biotite from a Sunrise Peak dike (sample # TJ-112), which presumably fed the flows and agglomerates between the two major lacustrine horizons, yielded a $^{40}Ar/^{39}Ar$ age of 35.3 $\pm$ 0.1 Ma. These ages are significantly older than the 32 m.y. age suggested by Morris and Lovering (1979) for these volcanic rocks, but they are in accordance with the recently determined ages of volcanic rocks found in adjacent ranges to the south and east (Witkind and Marvin, 1989; Le

Vot, 1984; Villien, 1984; Willis, 1986).

The upper lacustrine horizon may grade into an epiclastic sediment consisting of volcanic conglomerates and sandstones with a variety of latitic clast compositions (Plate 1). Due to the high porosity and carbonate content of the epiclastic sediments, hydrothermal fluids more completely altered these sediments compared to subjacent and overlying latite flows (Plate 2). However, in a few of the less-altered outcrops of this unit, abundant pumice (partly replaced by calcite) is interspersed with latite breccia. Some outcrops of this unit also contain a few angular clasts of Tintic Quartzite and other Paleozoic carbonates. The distribution and composition of this unit suggests it occurred near a sharp transition from a quiet lacustrine environment to a higher relief terrane with some Paleozoic rocks still exposed at the surface - possibly along a cladera wall.

Following deposition of the upper lacustrine unit ano the epiclastic sediments, widespread lava flows occurred, which ranged in composition from latite to shoshonite (Table 2). At least 6 flows can be distinguished in a few well exposed areas, but mapping individual flows is generally not possible due to the near identical composition of most flows. The reciprocal abundance of biotite versus orthopyroxone is perhaps the best field criteria we used for distinguishing the biotite latite flow units from the orthopyroxene-bearing mafic (or shoshonite) flows, which contain only traces of oxidized, resorbed biotite. Both units contain abundant clinopyroxene, plagioclase, and titanomagnetite and are clearly genetically related.

In addition, the distribution and thickness of these flows (and sedimentary units) may be controlled to some extent by an earlier-formed caldera (possibly related to eruption of the tuff member of the Copperopolis Latite).

For example, the mafic flows pinch out to the northeast of our mapped area, but thicken dramatically to the southwest (Plate 1). Lindgren and Loughlin (1919) described the occurrence of olivine basalt dikes west of Tintic Mountain while Morris and Lovering (1979) stated that they failed to find any evidence of this lithology. Lindgren and Loughlin (1919) report a partial chemical analysis of a flow near Buckhorn Mountain which is more alkaline and mafic than any rocks found by Morris and Lovering (1979), but is chemically similar to the mafic flows we have analyzed (Table 2).

Several vitrophyre horizons were located at the base of some of the biotite latite flows and were extensively sampled. Contrary to previous descriptions of these rocks, we found that many of the fresh flows and vitrophyres also contained phenocrystic amphibole and magmatic sulfide blebs. The occurrence of amphibole in some flows or samples and its absence in others is analogous to the reciprocal abundance of biotite and orthopyroxene. For example, the amphibole often occurs as overgrowths on, or as partial ("fibrous") replacements of, clinopyroxene. In other instances, clinopyroxene is found as a reaction rim on amphibole; the more oxidized or degassed lavas less commonly contain amphibole. These relationships suggest that amphibole occurred only late in the crystallization sequence and was often removed from the magma during degassing.

The biotite latite dikes have essentially the same chemical and modal composition as the biotite latite flows, including the occurrence of amphibole and magmatic sulfide blebs (discussed later). The dikes are classified as latite due to the extremely fine-grained texture of the groundmass. Inasmuch as most of the flow and lacustrine units dip about 20^{o} to the southeast, these dikes are progressively eroded to a deeper level going from the southeast to

the northwest portion of our mapped area. As this is done, the groundmass texture of the dikes becomes coarser grained. This transition along some dikes includes a change to Silver City Monzonite. Near this transition, the latite or monzonite oftens contains fragments or blocks (up to 3 m) of Tintic Quartzite. The biotite latite dikes often contain broken phenocrysts and strong flow foliation due to rapid eruption rates; the Silver City Monzonite may have been a more passively emplaced comagmatic draught, which accounts for the numerous stopped blocks in the Silver City Stock (Morris and Lovering, 1979) and in satellite intrusions which we mapped.

The field evidence for correlating the biotite latite dikes and the Silver City Stock as being comagmatic is supported by the $^{40}Ar/^{39}Ar$ ages of each unit. For example, a "vitrophyre" sample (TJ-84) from a vent facies biotite latite dike exhibits an age of 34.5 $\pm$ 0.2 Ma. Our plateau age for biotite from the Silver City Stock (sample HS-UTH-86-2; courtesy of J. Hannah) is only slightly younger, 33.6 $\pm$ 0.2 Ma (Tables 8 and 9; Figure 7).

Monzonite porphyry of Silver City Stock lithology extends south and east (Figure 1; Plate 1) across most of our mapped area. The correlation of these intrusions with the Silver City Stock is tentatively made on the basis of similar modal compositions and textures. Morris (1975) located some of these intrusions, but classified most of them as monzonite of Sunrise Peak lithology. The major element compositions of these two monzonites are essentially indistinguishable (Table 2). The apparent traditional criteria for distinguishing these two lighologies appears to be based on the occurrence of amphibole and a coarser-grained groundmass in the Silver City Monzonite. The problems with using this classification scheme will be discussed later.

Near the extreme southern end of our mapped area on the east flank of

Tintic Mountain, a dome or neck of feldspar porphyry was encountered. This lithology is identical in chemical and mineralogical composition to the descriptions of Lindren and Laughlin (1919) of the rhyolite of Tintic Mountain. In addition, it is chemically almost identical to the Swansea Quartz Monzonite and the Packard Quartz Latite (Table 2). Its most obvious characteristics are large Carlsbad-twinned sanidine phenocrysts (up to 3 cm) and an absence of any phenocrystic quartz. Smaller phenocrysts of plagioclase and minor biotite, oxyhornblende, titanomagnetite, and traces of magmatic pyrrhotite are also present. Lindgren and Laughlin (1919) stated that this lithology occurs on the west flank of Tintic Mountain, whereas the largest outcrop we found is on the east flank. However we did find one small intrusion on the west flank (Plate 1) which is nearly correlative in modal composition, but contains a slightly higher proportion of biotite and oxidized relict amphibole. We informally refer to this unit as the rhyolite of Keystone Springs to avoid use of the term "Tintic Mountain" which has been widely applied to other lithologies. Water-clear sanidine from this unit yielded a $^{40}Ar/^{39}Ar$ age of 34.1 $\pm$ 0.1 Ma (Figure 7, Tables 8 and 9).

Hydrothermal Alteration

Within the mapped area, an extensive area of hydrothermally altered volcanic rocks occurs which is approximately coincident with a swarm of dikes and small intrusions of Silver City Monzonite lithology (Plate 2). No previous maps or reports have deliniated or described the alteration, probably because of the apparent lack of nearby mineralization. However, the character of the alteration exhibits several similarities to the well-studied alteration in the East Tintic District that is present around productive intrusions (Lovering, 1949) and, consequently, merits some description and analysis.

The hydrothermal alteration was apparently structurally and chemically

controlled in several ways. The poorly welded tuff member of the Copperopolis Latite (at the base of the stratigraphic section) exhibits a pervasive argillic alteration. Whether or not the argillic alteration is zoned exclusively around monzonite intrusions or is related in part to fractures and faults is not well known. The high porosity and permeability of the tuff apparently allowed wider dispersal of alteration than occurred in other rock types.

The most obvious zonation of hydrothermal alteration is caused by stratigraphic changes in lithology. For example, immediately above the argillically altered tuff member of the Copperopolis Latite, the sediments of the lower member of the Golden's Ranch Formation commonly record a distinct change in alteration products. The lowest few meters of shale generally show strong argillic alteration. However the intensity of argillic alteration decreases upward in the section while the amount of pyrite and sericite present in the sediments rapidly increases. The greater amount of pyrite deposited in the sediments appears to be related to an increased carbonate content or porosity of a particular bed. Coincident with this change, some silicification of the most carbonate-rich beds occurs (although no jasperoid has yet been found in this unit). None of this alteration appears to be zoned around veins.

The flow and agglomerate member of the Copperopolis Latite that overlies the pyrite-rich lower member of the Golden's Ranch Formation typically exhibits alteration products indicative of less acidic conditions. The characteristic light green color of this unit (when altered) is imparted by abundant chlorite (replacing matrix and phenocryst constituents) and contrasts with the kaolinite-dominant assemblage of the underlying tuff member (Kim, 1988). The flows which clearly vented from Sunrise Peak almost always exhibit this type of propyllitic (or chloritic) alteration. This difference, in the dominant alteration products, probably is not due to original differences in

composition of these latitic units, inasmuch as these associations have been noted to be reversed in some outcrops of these units. Another common alteration characteristic of the agglomerate member is that quartz (clear euhedra) and calcite often line vugs and cavities while sparse limonite (after pyrite) occurs along fractures or small veinlets.

The alteration present in the upper lacustrine unit is more variable in intensity than the alteration present in underlying units. The shaley part of this unit is rarely exposed; however, one outcrop reveals that the basal part (~0.5 m) of the black, organic-rich shale contains abundant limonite, whereas the shale immediately above remains fresh and black (Figure 3). The lateral transition from limestone to jasperoid is also often abrupt (although recrystallization of the limestone may be more widespread). The most common variety of jasperoid found in this horizon is dense and black; however, various colors and porosities of jasperoid exist as well as variable amounts of interspersed limonite. Reflected light microscopy of vuggy, limonite-rich jasperoid reveals the presence of pyritohedral pyrite. Limestone adjacent to jasperoid generally exhibits evidence of substantial dissolution. The lateral variations in the alteration of this unit are probably related to proximity to hydrothermal conduits such as veins, faults, or dike margins.

Wide, persistent fissure veins generally occur in the more brittle (or reactive) rock types (such as the Paleozoic lithologies and porphyry intrusions). Consequently, significant veins have not been found in tuff, agglomerate, or lacustrine lithologies. However, one small vein (15 cm wide) occurs in agglomerate unit near Jumpoff Spring and exhibits a mineralogy consisting of quartz-calcite-dolomite-Fe-Mn-carbonates-barite-pyrite. With the exception of the carbonates, these gangue minerals are generally typical for many of the Tintic fissure veins. Other fragments of weathered vein material (also from

veins approximately 10-15 cm wide with variable proportions of quartz and carbonates) occur as float in the general vicinity of Jumpoff Spring, but soil cover prohibits determination of their exact location. No veins of this width have been found that cut the lacustrine units.

DISCUSSION

Magma Evolution and Volatile Fugacities

An important reason for examining the magmatic evolution and volatile fugacities of the parent magma chamber is to determine any special evolutionary processes which may have been important in the eventual formation of the ore. For example, the younger biotite latites apparently contain a higher proportion of magmatic sulfides which may have degassed to help form the ore fluid. The compositions of the individual mineral phases in the biotite latites flows and dikes and the Silver City Monzonite are unremarkable by themselves, but are generally equivalent; this reinforces the comagmatic interpretation suggested by the field relations and modal compositions. For example, the compositions of the clinopyroxenes in the flows, dikes, and monzonite of Silver City lithology are identical (Figure 6; Table 3). Although only a few analyses for plagioclase are available, the same corespondency is apparent (Table 4).

The compositions of the amphiboles from two widely seperated intrusions of Silver City Monzonite are also compared. One intrusion is adjacent to the concealed Cu-Mo deposit on the western side of the mapped area (Figure 1; Plate 1). The sample analyzed (TJ-164) has been intensely altered to the point that the stable mineral assemblage consists of epidote and amphibole. Amphibole from a comparatively fresh intrusion (TJ-153) exhibits an identical composition (Table 5). According to the classification scheme of Leake (1978), this composition is magnesio-hastingsite - a term chosen to point out the comparatively Mg-rich composition. By comparison, the biotite present in the latite flows is relatively Mg- or phlogopite-rich (59-65 mole % phlogopite) as might be expected (Table 6). This accounts for the reciprocal occurrence of biotite and amphibole versus orthopyroxene (and sanidine) in the

lavas (as also noted by Lindgren and Laughlin, 1919). Mg in the magma is incorporated in one of these three phases depending on the T, fO_2, fH_2O, and composition of the magma. It is difficult to isolate which variable is most important in preserving amphibole as a phenocrystic phase (see Rutherford et al., 1985) in some of the upper biotite latite flows and the Silver City Stock. However, the most likely cause may have been a gradually increasing water content of the magma. This may have also played a role in providing an extended episode of magmatic degassing to feed a hydrothermal ore fluid. However, Rutherford et al. (1985) speculate that the presence of sulfur also may help to preserve amphibole in a magma.

A trend towards more water-rich magmas with time would also increase the solubility of S in the magma by increasing the relative proportion of H_2S versus other sulfurous gases (Table 7).

Magmatic Sulfides

Immiscible sulfide blebs in intermediate to silicic magmas are probably quite common prior to eruption, but are generally either overlooked in chilled vitrophyres or they are removed during degassing of more slowly cooled lavas, tuffs, or intrusions. Hildreth (1977) noted magmatic pyrrhotite 1-10 microns in diameter sequestered within silicate and oxide phases from the Bishop Tuff. Whitney and Stormer (1983) and Drexler (1982) found pyrrhotite blebs of about the same dimensions within phenocrysts of the Fish Canyon Tuff and volcanic rocks of the Julcani district, Peru, respectively. Recently, we have documented the occurrence of magmatic sulfides in two additional volcanic complexes; namely, the Central Nevada Caldera Complex and the Salt Creek vent-facies dike in central Utah (Keith, unpublished data).

The results of our mapping reveals that monzonite intrusions of the productive Silver City lithology are far more wide-spread to the east and south of the stock (compare Figure 1A and 1B) than previous maps have indi-

cated (Morris, 1975). Monzonite intrusions near the southern part of the mapped area begin to give way to biotite latite dikes (along the same zones of emplacement) as the paleosurface at the time of intrusion is approached. Some portions of these biotite latite dikes were chilled rapidly enough that glass (now variably hydrated or devitrified) was preserved. These glassy or microcrystalline samples contain the highest proportion of magmatic sulfides. The reason for this unusual sulfide preservation may have been because the dikes were chilled, but not lowered completely to atmospheric pressure. By analogy, quenched glasses from submarine basalts (> 1000 m water depth) are notable for preserving high sulfur contents and sulfide globules indicative of magmatic conditions.

Magmatic sulfides from the East Tintic Mountains exhibit numerous similarities in mineralogy, morphology, and exsolution to those found in submarine basalts and in calc-alkaline rocks. Mathez (1976) surveyed the magmatic sulfide content of submarine basalt glasses from many localites; he found that the most sulfide rich sample contained sulfide globules up to 100 microns in diameter with a total modal sulfide abundance of about 0.01%. The most sulfide-rich biotite latite glass from the East Tintic Mountains which we have found so far contains globules up to 450 microns in diameter with a modal abundance of 0.02% (Figure 4). Careful modal analysis of the sulfide distribution in one sample revealed a total of 465 sulfide blebs over 1 micron in size in one thin section. Titanomagnetite contained 36% of the blebs, clinopyroxene contained 27%, the matrix 22%, biotite 10%, and plagioclase contained only 4%. The associated glass has S concentrations (~400 ppm) anticipated for sulfide saturation of this bulk composition (Carroll and Rutherford, 1985).

Sulfide Mineralogy, Exsolution Textures, and Degassing Processes

Petrographic examination of these sulfides has revealed several exsolution and degassing processes which may be related to the birth of a sulfide-rich ore fluid. Some of these include:

1) Early separation of a Cu-Fe-S phase (ISS) from the sulfide bleb at high temperatures. These exsolved ISS blebs form a scalloped margin around the parental monosulfide grain, line interior fractures (Figure 4A), or occur as a single discreet grain bounded by a curved surface (Figure 4F). [Hildreth (1977) also found Cu-rich margins on the much smaller pyrrhotite grains in the Bishop Tuff.]

2) Down-temperature the ISS phase exsolves chalcopyrite and very minor cubanite (Figure 4F).

3) The remaining Ni-Co-Ag-bearing pyrrhotite is often heterogeneous in Ni content (Figure 5). This may be related to a migration process analogous to pentlandite exsolution. Pyrite formed from the pyrrhotite during quenching, oxidation, or H_2S degassing also exhibits highly variable trace element content.

4) Pyrrhotite blebs are rarely preserved unless they are embedded: 1) near the centers of silicate phenocrysts (which are devoid of cracks to the crystal surface), 2) within titanomagnetite devoid of oxidation exsolution (or maghemitization) or 3) within some glomeroporphyritic clots (Figure 4). This may be due in part to the fact that S-rich pyrrhotite compositions spontaneously exsolve upon quenching, as noted by Craig and Scott (1974). Evidence for this process was also encountered by Whitney (1984) after examination of pyrrhotite blebs in the Fish Canyon Tuff. However, the most common process of

pyrrhotite removal evident in Tintic samples and the Fish Canyon Tuff is by reaction with oxygen (or loss of S) to produce pyrite and Fe-oxide (Figure 4). It is noteworthy that S (and Ag ??) migrates to the margins of the crystal (possibly along a prefered crystallographic direction (relict {0001} planes ?) in hexagonal pyrrhotite) while Fe, Co, and Ni show evidence for much less mobility during this degassing process. Perhaps partly as a consequence, Co and Ni are not important constituents in Tintic ores.

5) Sulfide blebs which are not protected by being sequestered in other phenocrysts or phenocryst clots show abundant evidence of resorption and disaggregation (Figure 4E) which would be expected during the depressurization involved with emplacement in shallow dikes and lavas. It is remarkable that any relict blebs are preserved in the matrix.

6) Both sulfide resorption and degassing might be aided by the presence of a saline magmatic fluid. Trace amounts of Na, K, Al, and Si present in the degassed portions of sulfide blebs might represent the deposition of alkalis and silica (in a feldspar or scapolite component) during solution of the S (and solution of Fe if it is in the P-T range for the retrograde solubility of Fe chloride; Whitney et al., 1985).

It is notable that these biotite latite dikes exhibit no halos of sulfide-rich alteration in the country rock; however, their more-slowly cooled monzonite counterparts exhibit large sulfide-rich argillic-phyllic alteration halos (Figure 1; Plate 2). Consequently, the lack of magmatic sulfides in the monzonite is due to the fact that they degassed during slow cooling in the presence of magmatic fluid and the S, As, and some of the metals were depo-

sited in the adjacent country rock. Some samples intermediate in texture between latite and monzonite exhibit spherical "spongy" Fe oxides where >90 % of the magmatic sulfur has been removed by degassing (and hydrothermal ?) processes. It was Lindgren and Loughlin (1919) who first confidently proposed that these monzonite dikes and intrusions are the ultimate source of the base- and precious-metal deposits in these districts. However, the discovery of abundant Cu- and Ag-bearing magmatic sulfides may be important evidence for their model.

The unusually large size of the Tintic sulfide blebs suggests that possibly rapid magma chamber convection combined with a prolonged presence of the immiscible sulfide phase in the magma chamber may have allowed efficient collection of those base- and precious-metals which have a high partition coefficient for a sulfide melt (i.e. Au, Ag, Cu, Ni, Co, and platinum-group elements (PGE)).

Initial microprobe analysis of the Tintic sulfides indicate the expected high concentrations of Ni (max. of 0.96 wt. % and ave. of 0.40 wt. %) and Co (max. of 0.51 wt. % and ave. of 0.14 wt. %); however, the weighted average Cu and Ag contents of the sulfides may be particularly high (Cu max. of 34.7 wt. % and ave. of 5.50 %; Ag max. of 0.03 % and ave. of < 0.01 %) when compared to magmatic sulfides from other systems. The difficulty with even attempting to make such comparisons is that very little quality analytical data for trace elements in magmatic sulfides from silicic to intermediate rocks is available. For example, the only data available for magmatic sulfide compositions for host rocks of this silica content (~ 59% SiO_2) and Fe/Mg ratio are from the magmatic sulfide ores at Sudbury, Ontario; the average Cu/Ni ratio for the Tintic magmatic sulfides (~15) is much higher than similar estimates for Sudbury (~0.7 - 1.0) (Naldrett, 1984). In addition, our initial Tintic sul-

fide data suggest that the Ag and As content may be distinctly higher than any Sudbury sulfides, but not enough data are yet available to confirm this assertion.

Sulfur-Rich Magmas

A critical question that needs further study is why some units in a volcanic sequence are more sulfide-rich than others. For example, some Tintic biotite latites are clearly abnormally enriched in magmatic sulfides. High sulfur content may in part be inherited from subduction and partial melting of sulfide-rich oceanic crust (Whitney and Stormer, 1983). Alternatively, magma mixing may cause perturbations in S and O fugacities or FeO content sufficient to nucleate magmatic sulfides which are then concentrated by crystal settling (as suggested by many authors for sulfide-rich zones in layered intrusions). In addition, the solubility of S in a mafic melt is much grater than in a more silicic melt; consequently, a magma mixing scheme whereby sulfide saturated mafic magma (such as the mafic flows described in this report) mixes with more differentiated magma may create an unusually high amount of magmatic sulfides. A third possibility is the introduction of crustal sulfur into the magma chamber by means of assimilation of sulfur-rich crustal rocks. Naldrett (in press) suggests that this process is critical to the formation of abundant magmatic sulfides in virtually all Cu-Ni deposits hosted by mafic intrusions with up to 75% of the sulfur and 50% of the magma being derived from assimilation of sulfate-rich (evaporites) country rocks. In terms of sulfur-rich volcanic rocks, Luhr et al. (1982) originally proposed a similar origin for the high sulfur content of the El Chichon volcanic rocks.

Some evidence from inclusions in the East Tintic latites suggests that assimilation of evaporites may have played a role in the formation of abundant magmatic sulfides. Our preliminary work found that one inclusion (which

exhibits weak relict layering ?) which is present in a latite flow with abundant magmatic sulfides consists dominantly of hercynite and potassium feldspar and very minor magmatic sulfide blebs. The presence of hercynite precludes a magmatic origin for the inclusion; however it may represent a metamorphosed fragment of the gypsiferous Arapien Shale which may underlie both the volcanic complex and subjacent thrust sheets in this area (and may be almost 1 km thick) and form part of the country rock around the parent magma chamber.

The isotopic signature of sulfides derived from sulfates would be very distinct from those formed by juvenile sulfur. Prior work on the S isotopic signatures of Tintic ores suggest values near -1.4 permil (Ames, 1970). Consequently, assimilation of evaporites would not appear to be an important contributor to the magmatic sulfides and subsequent hydrothermal ores. However, even minor assimilation of gypsiferous wallrocks may have kept the magma chamber near sulfide saturation over protracted episodes of fractionation and magma mixing. A sulfur isotope investigation of Tintic magmatic sulfides would help evaluate sources of sulfur and the potential buffering influence of evaporites on sulfide saturation.

Two of our initial analyses of these sulfide-rich rocks show elevated concentrations of Pd (TJ-83 with 110 ppb; TJ-84 with 93 ppb; courtesy of Geochemical Services Inc., Rocklin, CA). More work needs to be done to verify or refute these anomalies. However, elevated Pd concentrations in rocks which contain significant magmatic sulfides is not unexpected. Immiscible sulfide melts have particularly high partition coefficients for the PGE (platinum group elements). If magmatic sulfides are enriched in some draughts of magma by "crystal" settling, then some intrusions or lavas may show slightly elevated PGE contents as well as abundant sulfides. [No comparable Pt analyses

have been completed yet, but sub-equal amounts of Pt would be expected considering the small amount of magmatic fractionation which generally occurs between Pd and Pt.]

Potential Precious-Metal Mineralization

There are several reasons to suspect that the central East Tintic Mountains have limited potential for concealed Ag-Au deposits hosted by the Tertiary sediments, but substantial potential for mineralization hosted by underlying Paleozoic rocks. A short summary of these reasons are presented below.

1. Reactive Character of Tertiary Sedimentary Rocks. The previously unrecognized Tertiary sedimentary rocks we have found in the central East Tintic Mountains are often either pyrite-rich or contain some jasperoid. These characteristics indicate that these sediments reacted to hydrothermal solutions much the same as Paleozoic sedimentary rocks in the Tintic District. In addition, the jasperoids investigated contain pyritohedral pyrite which, according to Lovering (1949), is indicative of alteration assemblages close in time and space to mineralization.

2. Alteration Assemblages Analogous to Those in East Tintic District. Both the mineralogy and zonation of alteration present in the Government Canyon area are strongly similar to the early-barren, mid-barren, and late-barren alteration stages of Lovering (1949; Figure 1). This evidence indicates that the alteration present in the Government Canyon probably formed at the same general time as that present in the Tintic and East Tintic Districts.

3. Northeast Alignment of Biotite Latite Dikes. A general northeast trend of some the biotite latite dikes is present in the central East Tintic Mountains (Figure 1; Plate 1). This may represent a deepseated zone of structural weakness that guided emplacement of the high-level

intrusions and persisted during subsequent hydrothermal events, simlar to the East Tintic District.

4. Shallow Levels of Erosion. Inasmuch as the central East Tintic Mountains represent an eastward dipping fault block (Figure 3), the current level of erosion in Government Canyon is less than that present to the west (and north?) where the productive interval of veins intersected the surface. Structural intersections and lithologies favorable to mineralization may be present at depths feasible for mining in Government Canyon.

5. Presence of Productive Intrusions. Intrusions in the central East Tintic Mountains were previously thought to be of the barren Sunrise Peak lithology; however, our work demonstrates that many of them are amphibole-bearing and are probably satellitic plugs of the Silver City Stock. The high level expression of these intrusions are biotite latite dikes which are rich in magmatic sulfides with detectable Ag. Degassing of such magma could produce a viable ore fluid.

6. Potential East-West Zonation in Au/Ag Ratio. Many mining districts exhibit a pattern of increasing Au/Ag ratios in veins with increasing distance from an intrusive center. Considering the occurrence of disseminated Cu-Mo mineralization and Pb-Ag veins a short distance west of Government Canyon (Figure 3), any mineralization that may have formed from the same hydrothermal system in Government Canyon might have a higher precious metal content.

7. Abundant Structural Sites For Ore Deposition. Structural preparation of the ground (via normal faults and thrusts) has long been recognized as an integral necessity for significant mineralization in these districts. Contrary to the mapping of Morris (1975), several major faults offset the

volcanic and lacustrine units in Government Canyon (Plate 1). In addition, jasperoid and silicified volcanic rocks have been found close to inferred intersections of these faults which suggests that they were used as hydrothermal conduits.

8. Potential For Paleozoic Carbonate-Hosted Replacement Deposit. Due to the moderate-to-high topographic relief that was present along this portion of the thrust belt prior to volcanism, it is impossible to accurately predict the thickness of the volcanic cover from surface mapping alone (as drilling in the East Tintic District indicates). A weakly mineralized fracture or seam in volcanic rocks is often the only surface expression of a major replacement ore deposit in the underlying carbonate rocks in the East Tintic District (Gillerman, 1986). This might justify further exploration in the central East Tintic Mountains along weakly mineralized fissure veins where the thickness of the volcanic cover is not well constrained. Particularly compelling would be the search for a shallowly buried caldera wall in a area of intense hydrothermal alteration or productive intrusions.

9. Potential For "Porphyry-Hosted" or Diatreme Precious Metal Deposits. There are several good reasons to suspect that the occurrence of a variant of the porphyry-hosted or diatreme precious metal deposit is at least a possibility in central Utah. The general type of deposit included under these headings are those associated with alkalic intrusions or volcanic centers such as the Allard stock in Colorado, alkaline porphyry Cu-Au deposits in British Columbia or other diatreme-maar Au deposits in the western U.S. (Werle et al., 1984; and many others). Clearly, the rocks we have investigated to date in central Utah are not as alkalic as the host rocks for many of these deposits. However, it is interesting to

note that the Allard Stock is described as containing "immiscible sulfides" in one of the intrusive units. It also exhibits a Pd content identical to the Tintic biotite latite dikes as well as subeconomic Cu mineralization (Werle et al., 1984). The occurrence of tellurides in Tintic and East Tintic ores, moderately alkalic rocks (such as the syenites, monzonites, and trachytes of the Salt Creek - Levan areas), and a few large breccia pipes in the East Tintic Mountains (and adjacent areas; Morris and Morgensen, 1978; Morris, 1975; Keith, unpublished data) is at least permissive evidence in favor undiscovered breccia- or diatreme-hosted Au-Ag telluride deposits existing in central Utah. The most important facet in conducting exploration for this type of deposit is locating areas of maximum structural disruption (breccia pipes, diatremes, volcanic vents) that coincide with strong alteration in the central East Tintic Mountains. It is certainly possible that lacustrine sediments are partially filling or covering latitic maars or vents of the Copperopolis episode. In addition, the lacustrine sediments may have served as a barrier and roof to some Sunrise Peak breccia pipes as well as intrusions. However, far more detailed mapping and sampling (and drilling) is needed to examine these possibilities.

CONCLUSIONS AND SUMMARY

This report documents several new findings concerning the geology and mineral potential of the central East Tintic Mountains, Utah. For example, fission-track ages and $^{40}Ar/^{39}Ar$ ages which we report suggest that some of the volcanism in this area which is contemporaneous or stratigraphically beneath the lacustrine horizons is as old as ca. 37.4 to 35.3 Ma (Figure 7). Age determinations for units above the lacustrine horizons (or for intrusions which cut them) range from 34.5 to 33.6 Ma. This implies that a large caldera related to the eruption of the younger Packard Quartz Latite and Fernow Quartz Latite is not present in this area. However, our data suggests that a smaller caldera related to the eruption of the tuff member of the Copperopolis Latite may be present. We note that many monzonite dikes and intrusions in this area are hornblende bearing and are correlative in modal and chemical composition with the productive Silver City Stock rather than the barren Sunrise Peak Stock. The large areas of hydrothermal alteration which surround these intrusions exhibit many similarities to the well-studied alteration halos in the East Tintic District. The age, composition, and field relationships of the post-lacustrine volcanic rocks suggest that they may represent, in part, the extrusive equivalents of the monzonite dikes and Silver City Stock. Our work suggests that the Silver City Stock and related intrusions may be part of one of the youngest (33.6 $\pm$ 0.2 Ma) igneous events in the central East Tintic Mountains, but not as young as previously suggested (ca. 31.5 Ma).

In addition, our recent work has documented the existence of unusually large (and abundant) <u>magmatic</u> sulfides in lava vitrophyres and vent-facies biotite latite dikes, which are the surface expressions of the Silver City Quartz Monzonite intrusions in this area. In addition, preliminary analytical

data suggest that the sulfides host most (~75%) of the Ag present in the latites. The East Tintic Mountains are potentially the first locality, world-wide, where Ag in mesothermal veins can be demonstrated to be derived from degassed Ag-bearing magmatic sulfides. Consequently, the central East Tintic Mountains are a favorable area for exploration for Ag (Pb-Zn-Cu-Au) ore bodies because: 1) productive monzonite intrusions are present, and 2) Paleozoic rocks favorable for ore deposition may be present beneath relatively thin volcanic cover because the area is <u>not</u> entirely enclosed within a caldera which hosts great thicknesses of barren volcanic rocks.

ACKNOWLEDGEMENTS

This study was funded in part by contract # 88-3548 with the Utah Geological and Mineral Survey. Their assistance is gratefully acknowledged. Discussions and field excursions with Glenn Mellor, Judy Hannah, Grant Willis, Eric Christiansen, Mark Jensen, Mike Shubat, and Bob Gloin helped modify or formulate some of our ideas.

REFERENCES

Ballantyne, J. N., and Moore, J. N., 1988, Arsenic geochemistry in geothermal systems: Geochimica et Cosmochimica Acta, v. 52, p. 475-483.

Cabri, L. J., 1981, Relationship of mineralogy to the recovery of PGE from ores: in: L. J. Cabri, editor, Platinum-Group Elements: Mineralogy, Geology, Recovery, CIM Special Volume 23, p. 233-250.

Carroll, M. R., and Rutherford, M. J., 1985, Sulfide and sulfate saturation in hydrous silicate melts: Journal of Geophysical Research, v. 90, suppl. C601-C612.

Coats, C. J. A., and Snajdr, P., 1984, Ore deposits of the North Range, Onaping-Levack area, Sudbury: in Pye, E. G., Naldrett, A. J., and Giblin, P. E., eds., The Geology and Ore Deposits of the Sudbury Structure, Ontario Geological Survey Special Volume 1, p. 327-346.

Craig, J. R., and Scott, S. D., 1974, Sulfide phase equilibria: in Ribbe, P. H., ed., Sulfide Mineralogy, Mineralogical Society of America Short Course Notes, v. 1, p. CS-1 to CS-110.

Distler, V. V., Genkin, A. D., and Dyuzhikov, O. A., 1986, Sulfide petrology and genesis of copper-nickel ore deposits: in Friedrich, G. H., Genkin, A. D., Naldrett, A. J., Ridge, J. D., Sillitoe, R. H., and Vokes, F. M., eds., Geology and Metallogeny of Ore Deposits, p. 111-123.

Drexler, J. W., 1982, Magmatic conditions from vitric units of the Julcani district, Peru: unpublished Ph.D dissertation, Michigan Technological University, Houghton, Michigan.

Einaudi, M. T., Moore, W. J., and Wilson, J. C., 1978, An issue devoted to the Bingham mining district: Economic Geology, v. 73, p. 1215-1217.

Hildreth, E. W., 1977, The magma chamber of the Bishop Tuff: Gradients in temperature, pressure, and composition: unpublished Ph.D. dissertation,

University of California - Berkeley.

Gillerman, V. S., 1986, Barren hot spring alteration versus precious metal related alteration, Tintic district, Utah: Geological Society of America Abstracts with Programs, v. 18, p. 614.

Keith, J. D., Dallmeyer, R. D., and Kowallis, B. J., 1989, Latite with magmatic pyrrhotite: A possible precursor to monzonite-related alteration/mineralization in the East Tintic Mountains, Utah: Geological Society of America Abstracts With Programs, v. 21, p. 100.

Keith, J. D., Kim, C. S., Dallmeyer, R. D., Kowallis, B. J., and Willis, G. C., in prep., Evaluation of the history of Eocene-Oligocene volcanism, sedimentation, and hydrothermal alteration in the central East Tintic Mountains, Utah: (for submission to the UGMS Miscellaneous Publication Series).

Keith, J. D., Shanks, W. C., III, Archibald, D. A., and Farrar, E., 1986, Volcanic and intrusive history of the Pine Grove porphyry molybdenum system, southwestern Utah: Economic Geology, v. 81, p. 553-577.

Kim, C. S., 1988, Geochemical aspects of Eocene-Oligocene volcanism and alteration in central Utah: unpub. M. S. thesis, University of Georgia, Athens, 106 p.

Kim, C. S., and Keith, J. D., 1989, Stratigraphically-controlled alteration related to sub-volcanic intrusions in the central East Tintic Mountains, Utah: Geological Society of America Abstracts With Programs, v. 21, p. 101.

Lightfoot, P. C., Naldrett, A. J., and Hawkesworth, C. J., 1984, The geology and geochemistry of the Waterfall Gorge section of the Insizwa complex with particular reference to the origin of the nickel sulfide deposits: Economic Geology, v. 79, p. 1857-1879.

Lindgren, Waldmar, and Loughlin, G. F., 1919, Geology and ore deposits of the Tintic mining district, Utah: U.S. Geological Survey Professional Paper 107, 282 p.

Lovering, T. S., 1949, Rock alteration as a guide to ore - East Tintic district, Utah: Economic Geology Monograph 1, 65 p.

Luhr, J., Carmichael, I. S. E., and Varecamp, J. C., 1982, Eruption of El Chichon volcano, Chipas, Mexico: EOS (Transactions of the American Geophysical Union), v. 63, p.1126-1127.

Mathez, E. A., 1976, Sulfur solubility and magmatic sulfides in submarine basalt glass: Journal of Geophysical Research, v. 81, p. 4269-4276.

Morris, H. T., 1975, Geologic map and sections of the Tintic Mountain quadrangle and adjacent part of the McIntyre quadrangle, Juab and Utah Counties, Utah: U.S. Geological Survey Map I-883.

Morris, H. T., and Lovering, T. S., 1979, General geology and mines of the East Tintic mining district, Utah and Juab Counties, Utah: U.S. Geol. Survey Prof. Paper 1024, 203 p.

Morris, H. T., and Morgensen, A. P., 1978, Tintic Mining district, Utah: Brigham Young University Geology Studies, p. 33-45.

Naldrett, A. J., in press, Sulfide melts: Crystallization temperatures, solubilities in silicate melts, and Fe-Ni-Cu partitioning between basaltic magmas and olivine: in Whitney, J. A., and Naldrett, A. J., eds., Ore deposition Associated with Magmas, Reviews in Economic Geology, v. 4.

Villien, A., 1984, Central Utah deformation belt: unpub. Ph.D. thesis, University of Colorado, 282 p.

Werle, J. L., Ikramuddin, M., and Mutschler, F. E., 1984, Allard stock, La Plata Mountains, Colorado--an alkaline rock-hosted porphyry Cu - precious metal deposit: Canadian Journal of Earth Science, v. 21, p. 630-641.

Whitney, J. A., 1984, Fugacities of sulfurous gases in pyrrhotite-bearing silicic magmas: American Mineralogist, vol. 69, p. 69-78.

Whitney, J. A., and Stormer, J. C., Jr., 1983, Igneous sulfides in the Fish Canyon Tuff and the role of sulfur in calc-alkaline magmas: Geology, v. 11, p. 99-102.

Whitney, J. A., Hemley, J. J., Simon, F. O., 1985, The concentration of iron in chloride solutions equilibrated with synthetic granitic compositions: The sulfur free system: Economic Geology, v. 80, p. 444-460.

Willis, G. C., 1985, Revisions to the geochronology and source areas of early Tertiary formations in the Salina area of Sevier Valley, central Utah: Geological Society of America Abstracts with Programs, v. 17, p. 272.

Willis, G. C., 1986, Geologic map of the Salina Quadrangle: Utah Geological and Mineral Survey Map 83.

Willis, G. C., 1987, The Late Eocene formation of Aurora, a replacement for the abandoned Bald Knoll Formation in the Seveir Valley area, central Utah: Geological Society of America Abstracts with Programs, v. 19, p. 343.

Witkind I. J., and Marvin, R. F., 1989, Significance of new potassium-argon ages from the Goldens Ranch and Moroni Formations, Sanpete-Sevier Valley area, central Utah: Geological Society of America Bulletin, v. 101, p. 534-548.

Wood, S. A., 1987, Thermodynamic calculations of the volatility of the platinum group elements (PGE): The PGE content of fluids at magmatic temperatures: Geochimica et Cosmochimica Acta, v. 51, p. 3041- 3050.

TABLE 1.

FISSION TRACK AGE DATA

Unit	Sample Number	Mineral Analyzed	Method	Location		No of Grains	Track Denisty $tr/ce^2 \ 10^5$		Neutron Dose $D/cm^2 \times 10^{14}$	Age ± Error (2σ)
				N. Lat.	W. Long.		Fossil	Induced		
Lower Member	TJ-6	Apatite	Pop.	39°51'11"	111°3'20"	150	1.30 (701)	2.44 (1315)	11.26 (3121)	35.8 ± 5.1 Ma
Upper Member	TJ-9	Apatite	Pop.	39°51'11"	111°3'20"	150	1.92 (1038)	3.44 (1860)	11.26 (3121)	37.5 ± 5.2 Ma

TABLE 2
WHOLE-ROCK MAJOR ELEMENT ANALYSES

Sample #	*	*	TJ-84	TJ-76	TJ-80A	TJ-80B
Lithology	Silver City Monzonite	Sunrise Peak Monzonite	Biotite Latite Dike	Upper Biotite Latite	Upper Biotite Latite	Upper Biotite Latite
Wt % Oxide						
SiO_2	61.08	60.13	59.02	59.41	58.68	60.83
TiO_2	0.89	0.89	0.94	1.01	0.99	0.99
Al_2O_3	16.14	16.19	16.64	16.60	16.22	17.51
Fe_2O_3	7.59	7.16	7.00	7.58	8.25	6.48
MnO	0.12	0.14	0.12	0.12	0.12	0.12
MgO	2.21	2.84	2.50	2.75	3.10	1.79
CaO	3.97	4.16	5.02	5.64	5.94	5.51
Na_2O	3.08	3.20	3.61	2.57	2.62	2.59
K_2O	4.50	4.88	4.55	3.90	3.64	3.72
P_2O_5	0.43	0.40	0.48	0.40	0.43	0.45
S	0.02	0.02	0.06	0.01	0.01	0.01
CIPW Norm						
Q	15.39	10.83	9.18	14.57	14.47	18.37
C	0.03	0.00	0.00	0.00	0.00	0.30
Or	26.58	28.81	26.91	23.04	21.49	21.96
Ab	26.03	27.09	29.81	21.64	22.13	21.87
An	16.87	15.42	16.14	22.30	21.77	24.41
Di	0.00	2.02	2.21	2.36	1.48	0.00
Hy	5.50	6.14	5.21	5.76	7.03	4.45
Mt	0.00	0.00	0.00	0.00	0.00	0.00
Il	0.21	0.26	0.25	0.27	0.27	0.26
Hm	7.59	7.16	7.00	7.58	8.25	6.48
Tn	0.00	1.83	1.99	2.14	2.09	0.00
Ru	0.78	0.00	0.00	0.00	0.00	0.85
Ap	1.02	0.95	1.13	0.96	1.03	1.06
Pr	0.04	0.04	0.00	0.00	0.00	0.00
Diff. Index	68.00	66.73	65.90	59.25	58.09	62.19

TABLE 2 (continued)
WHOLE-ROCK MAJOR ELEMENT ANALYSES

Sample #	TJ-8	TJ-64	TJ-75	TJ-77	*	*
Lithology	Lower Biotite Latite	Lower Biotite Latite	Rhyolite Of Keystone Springs	Rhyolite Of Keystone Springs	Swansea Quartz Monzonite	Packard Quartz Latite
Wt % Oxide						
SiO_2	60.39	58.47	71.49	70.45	71.63	70.86
TiO_2	0.93	0.99	0.42	0.42	0.42	0.40
Al_2O_3	16.24	17.47	14.92	15.55	14.73	15.42
Fe_2O_3	7.25	6.91	2.05	2.28	2.34	2.44
MnO	0.12	0.12	0.09	0.10	0.07	0.06
MgO	2.61	2.42	0.65	0.56	0.71	0.70
CaO	5.19	5.50	1.05	1.22	1.14	2.62
Na_2O	2.50	2.99	3.90	4.32	3.03	3.19
K_2O	4.30	4.61	5.35	5.02	5.82	4.17
P_2O_5	0.44	0.49	0.08	0.10	0.12	0.14
S	0.01	0.01	0.01	0.00	0.01	0.01
CIPW Norm						
Q	15.71	10.30	25.34	22.95	28.61	30.06
C	0.00	0.00	1.00	1.03	1.67	1.23
Or	25.39	27.23	31.61	29.64	34.37	24.63
Ab	21.05	25.06	33.01	36.54	25.60	27.02
An	20.45	20.78	4.66	5.43	4.88	12.10
Di	1.88	0.29	0.00	0.00	0.00	0.00
Hy	5.62	5.90	1.63	1.39	1.76	1.75
Mt	0.00	0.00	0.00	0.00	0.00	0.00
Il	0.26	0.27	0.17	0.21	0.13	0.11
Hm	7.25	6.91	2.05	2.28	2.34	2.44
Tn	1.70	2.08	0.00	0.00	0.00	0.00
Ru	0.09	0.00	0.33	0.31	0.35	0.34
Ap	1.05	1.16	0.19	0.23	0.29	0.32
Pr	0.00	0.00	0.02	0.00	0.02	0.02
Diff. Index	62.15	62.59	89.96	89.13	88.58	81.71

TABLE 2 (continued)
WHOLE-ROCK MAJOR ELEMENT ANALYSES

Sample #	TJ-108	TJ-18
Lithology	Upper Biotite Latite	Mafic flows
Wt % Oxide		
SiO_2	62.02	54.23
TiO_2	0.83	1.16
Al_2O_3	15.84	17.71
Fe_2O_3	6.45	8.46
MnO	0.09	0.14
MgO	2.51	2.57
CaO	4.37	7.69
Na_2O	3.10	3.46
K_2O	4.43	3.93
P_2O_5	0.36	0.57
S	0.12	0.04
CIPW Norm		
Q	15.62	3.57
C	0.00	0.00
Or	26.15	23.24
Ab	26.21	28.66
An	16.26	21.51
Di	0.08	7.34
Hy	6.23	2.99
Mt	0.00	0.00
Il	0.00	0.29
Hm	6.45	8.46
Tn	2.12	2.46
Ru	0.00	0.00
Ap	0.85	1.35
Pr	0.21	0.00
Diff. Index	67.98	55.47

TABLE 3

PYROXENE ANALYSES

Sample #	TJ-84	TJ-84	TJ-84	TJ-84	TJ-84	TJ-93	TJ-83
Comment	Small	Core	Small	Small	Medium	CPX	CPX
Wt% Oxides							
SiO_2	50.87	50.37	51.67	51.40	51.43	51.60	50.97
TiO_2	0.64	0.77	0.35	0.35	0.31	0.40	0.52
Al_2O_3	3.17	3.89	1.60	2.01	0.40	1.98	2.29
Cr_2O_3	0.00	0.00	0.00	0.00	0.00	0.00	0.00
FeO	7.64	8.25	8.63	8.72	8.52	8.54	9.19
MnO	0.26	0.19	0.60	0.66	0.65	0.51	0.45
MgO	15.09	14.69	14.25	14.69	14.47	14.60	14.69
CaO	21.53	21.50	21.81	21.02	21.76	20.78	20.30
Na_2O	0.34	0.35	0.47	0.44	0.41	0.43	0.36
Total	99.54	100.01	99.38	99.29	98.95	98.84	98.77
Cations per 6 Oxygens							
Si	1.898	1.876	1.944	1.933	1.944	1.943	1.925
Ti	0.018	0.022	0.010	0.010	0.009	0.011	0.015
Al	0.139	0.171	0.071	0.089	0.062	0.088	0.102
Cr	0.000	0.000	0.000	0.000	0.000	0.000	0.000
Fe^{+2}	0.238	0.257	0.272	0.274	0.269	0.269	0.290
Mn	0.008	0.006	0.019	0.021	0.021	0.016	0.014
Mg	0.839	0.815	0.799	0.823	0.815	0.819	0.827
Ca	0.861	0.858	0.879	0.847	0.881	0.839	0.822
Na	0.025	0.025	0.034	0.032	0.030	0.031	0.026
Sum	4.027	4.030	4.028	4.029	4.031	4.017	4.022
Wo	0.444	0.444	0.451	0.436	0.448	0.435	0.424
En	0.433	0.422	0.410	0.423	0.415	0.425	0.427
Fs	0.123	0.133	0.139	0.141	0.137	0.140	0.150

PYROXENE ANALYSES

Sample #	TJ-83	TJ-84	TJ-84	TJ-89	TJ-89	TJ-89	TJ-89
Comment	CPX Core	Lrg CPX	Lrg CPX	Lrg CPX	Small CPX	Lrg	Lrg CPX
Wt% Oxides							
SiO_2	51.30	49.56	51.72	51.71	50.88	50.24	50.72
TiO_2	0.51	0.80	0.62	0.39	0.43	0.72	0.70
Al_2O_3	1.97	3.93	2.15	1.86	2.08	2.87	2.80
Cr_2O_3	0.00	0.00	0.00	0.00	0.00	0.00	0.00
FeO	9.07	7.56	8.26	8.04	8.71	7.66	7.86
MnO	0.49	0.30	0.45	0.45	0.45	0.26	0.38
MgO	14.95	13.98	15.23	14.84	14.74	14.97	14.96
CaO	20.49	22.21	20.65	21.44	20.62	21.47	21.18
Na_2O	0.40	0.38	0.39	0.36	0.39	0.34	0.34
Total	99.18	98.72	99.47	99.09	98.30	98.53	98.94
Cations per 6 Oxygens							
Si	1.930	1.872	1.931	1.941	1.930	1.897	1.906
Ti	0.014	0.023	0.017	0.011	0.012	0.020	0.020
Al	0.087	0.175	0.095	0.082	0.093	0.128	0.124
Cr	0.000	0.000	0.000	0.000	0.000	0.000	0.000
Fe^{+2}	0.285	0.239	0.258	0.252	0.276	0.242	0.247
Mn	0.016	0.010	0.014	0.014	0.014	0.008	0.012
Mg	0.838	0.787	0.848	0.830	0.833	0.842	0.838
Ca	0.826	0.899	0.826	0.862	0.838	0.869	0.853
Na	0.029	0.028	0.028	0.026	0.029	0.025	0.025
Sum	4.026	4.032	4.018	4.020	4.026	4.031	4.025
Wo	0.424	0.467	0.428	0.443	0.430	0.445	0.440
En	0.430	0.409	0.439	0.427	0.428	0.431	0.432
Fs	0.146	0.124	0.134	0.130	0.142	0.124	0.127

PYROXENE ANALYSES

Sample #	TJ-89	TJ-89	TJ-153	TJ-153	TJ-153	TJ-153	TJ-153
Comment	Lrg CPX	Mod CPX	CPX	Lrg XL	Lrg XL	Lrg Core	Margin
Wt% Oxides							
SiO_2	51.07	50.42	51.00	51.97	51.51	51.57	51.70
TiO_2	0.54	0.69	0.32	0.11	0.34	0.30	0.24
Al_2O_3	2.32	2.68	1.60	0.62	0.20	1.47	1.13
Cr_2O_3	0.00	0.00	0.00	0.00	0.00	0.00	0.00
FeO	7.52	7.76	9.50	9.08	8.77	9.32	8.97
MnO	0.39	0.30	0.36	0.70	0.50	0.39	0.45
MgO	15.25	14.93	14.28	13.75	14.58	14.49	14.35
CaO	21.14	21.23	21.07	22.09	21.28	20.83	21.10
Na_2O	0.33	0.34	0.36	0.24	0.31	0.37	0.38
Total	98.56	98.35	98.49	98.56	98.49	98.74	98.32
Cations per 6 Oxygens							
Si	0.923	1.906	1.940	1.976	1.953	1.951	1.963
Ti	0.015	0.020	0.009	0.003	0.010	0.009	0.007
Al	0.103	0.119	0.072	0.028	0.054	0.066	0.051
Cr	0.000	0.000	0.000	0.000	0.000	0.000	0.000
Fe^{+2}	0.237	0.245	0.302	0.289	0.278	0.295	0.285
Mn	0.012	0.010	0.012	0.023	0.016	0.012	0.014
Mg	0.856	0.841	0.809	0.779	0.824	0.817	0.812
Ca	0.853	0.860	0.859	0.900	0.865	0.844	0.859
Na	0.024	0.025	0.027	0.018	0.023	0.027	0.028
Sum	4.023	4.027	4.029	4.016	4.022	4.021	4.019
Wo	0.438	0.442	0.436	0.457	0.440	0.432	0.439
En	0.440	0.432	0.411	0.396	0.419	0.418	0.415
Fs	0.122	0.126	0.153	0.147	0.141	0.151	0.146

PYROXENE ANALYSES

Sample #	TJ-64	TJ-64	TJ-64	TJ-64	TJ-64	TJ-64	TJ-64
Comment	CPX	Same XL	Mod CPX	CPX	CPX Clot	Same Clot	Lrg in Clot
Wt% Oxides							
SiO_2	51.70	51.49	51.77	50.87	51.32	51.38	50.49
TiO_2	0.39	0.43	0.37	0.62	0.47	0.45	0.64
Al_2O_3	1.72	1.90	1.55	2.46	1.95	1.88	2.64
Cr_2O_3	0.00	0.00	0.00	0.00	0.00	0.00	0.00
FeO	8.39	8.27	8.42	8.11	8.47	8.37	8.41
MnO	0.52	0.44	0.54	0.49	0.58	0.57	0.49
MgO	14.58	14.69	14.57	14.79	14.46	14.53	14.09
CaO	21.59	21.47	21.82	21.31	21.29	21.18	21.59
Na_2O	0.42	0.39	0.39	0.38	0.40	0.40	0.42
Total	99.31	99.08	99.43	99.03	98.94	98.76	98.77
Cations per 6 Oxygens							
Si	1.942	1.936	1.944	1.914	1.935	1.939	1.910
Ti	0.011	0.012	0.010	0.018	0.013	0.013	0.018
Al	0.076	0.084	0.069	0.109	0.087	0.084	0.118
Cr	0.000	0.000	0.000	0.000	0.000	0.000	0.000
Fe^{+2}	0.264	0.260	0.264	0.255	0.267	0.264	0.266
Mn	0.017	0.014	0.017	0.016	0.019	0.018	0.016
Mg	0.816	0.823	0.815	0.829	0.813	0.817	0.794
Ca	0.869	0.865	0.878	0.859	0.860	0.856	0.875
Na	0.031	0.028	0.028	0.028	0.029	0.029	0.031
Sum	4.024	4.024	4.026	4.028	4.023	4.021	4.028
Wo	0.446	0.444	0.448	0.442	0.443	0.442	0.452
En	0.419	0.423	0.416	0.427	0.419	0.422	0.410
Fs	0.135	0.133	0.135	0.131	0.138	0.136	0.137

PYROXENE ANALYSES

Sample #	TJ-55	TJ-55	TJ-55	TJ-55	TJ-55	TJ-55	TJ-55
Comment	CPX	Mod CPX	Sml-Dek-XL	Mod-CPX	Mod-XL-Core	Lrg CPX	Zoned Rim
Wt% Oxides							
SiO_2	50.78	52.10	47.84	51.65	51.86	50.81	46.35
TiO_2	0.68	0.32	1.11	0.34	0.33	0.56	0.88
Al_2O_3	2.57	1.52	4.82	1.49	0.67	2.37	3.82
Cr_2O_3	0.00	0.00	0.00	0.00	0.00	0.00	0.00
FeO	8.09	8.56	8.73	8.17	8.29	8.72	8.48
MnO	0.50	0.59	0.18	0.67	0.68	0.60	0.29
MgO	14.63	14.86	13.31	14.59	14.98	14.50	13.21
CaO	21.65	21.16	22.02	21.43	21.43	21.16	23.41
Na_2O	0.38	0.40	0.32	0.40	0.37	0.41	0.27
Total	99.28	99.51	98.33	98.74	99.61	99.13	96.71
Cations per 6 Oxygens							
Si	1.908	1.951	1.827	1.950	1.941	1.916	1.816
Ti	0.019	0.009	0.032	0.010	0.009	0.016	0.026
Al	0.114	0.067	0.217	0.066	0.074	0.105	0.176
Cr	0.000	0.000	0.000	0.000	0.000	0.000	0.000
Fe^{+2}	0.254	0.268	0.279	0.258	0.259	0.275	0.278
Mn	0.016	0.019	0.006	0.021	0.022	0.019	0.010
Mg	0.819	0.829	0.758	0.821	0.835	0.815	0.771
Ca	0.872	0.849	0.901	0.867	0.859	0.855	0.983
Na	0.028	0.029	0.024	0.029	0.027	0.030	0.021
Sum	4.030	4.021	4.044	4.022	4.026	4.031	4.080
Wo	0.448	0.436	0.465	0.446	0.440	0.440	0.484
En	0.421	0.426	0.391	0.422	0.428	0.419	0.380
Fs	0.131	0.138	0.144	0.133	0.133	0.141	0.137

PYROXENE ANALYSES

Sample #	TJ-55	TJ-64	TJ-64	TJ-92A	TJ-92A	TJ-92A	TJ-92A
Comment	Core	Core	Lrg CPX	Core	Core	Mod-Size XL	Part of Lrg XL
Wt% Oxides							
SiO_2	50.50	51.13	51.78	52.50	53.77	51.72	54.12
TiO_2	0.60	0.55	0.39	0.20	0.12	0.32	0.13
Al_2O_3	3.00	2.17	1.45	1.08	0.66	1.46	0.63
Cr_2O_3	0.00	0.00	0.00	0.00	0.00	0.00	0.00
FeO	9.51	8.13	8.03	8.53	17.43	8.11	17.17
MnO	0.58	0.62	0.56	0.64	1.08	0.49	1.00
MgO	13.88	14.82	15.19	14.75	25.34	15.00	25.42
CaO	21.26	20.97	21.02	21.11	1.11	21.32	1.14
Na_2O	0.44	0.36	0.37	0.35	0.02	0.35	0.03
Total	99.77	98.75	98.79	96.16	99.53	98.77	99.64
Cations per 6 Oxygens							
Si	1.899	1.928	1.949	1.971	0.975	1.949	1.981
Ti	0.017	0.016	0.011	0.006	0.003	0.009	0.004
Al	0.133	0.096	0.064	0.048	0.029	0.065	0.027
Cr	0.000	0.000	0.000	0.000	0.000	0.000	0.000
Fe^{+2}	0.299	0.256	0.253	0.268	0.535	0.256	0.526
Mn	0.018	0.020	0.018	0.020	0.034	0.016	0.031
Mg	0.778	0.833	0.852	0.825	1.387	0.842	1.387
Ca	0.857	0.847	0.848	0.849	0.044	0.861	0.045
Na	0.032	0.026	0.027	0.025	0.001	0.026	0.002
Sum	4.033	4.022	4.021	4.012	4.008	4.023	4.003
Wo	0.443	0.438	0.434	0.437	0.022	0.439	0.023
En	0.402	0.430	0.436	0.425	0.705	0.430	0.709
Fs	0.155	0.132	0.129	0.138	0.272	0.130	0.269

PYROXENE ANALYSES

Sample #	TJ-92A	TJ-92A
Comment	Small CPX	Small OPX
Wt% Oxides		
SiO_2	49.90	53.07
TiO_2	0.76	0.15
Al_2O_3	3.14	0.66
Cr_2O_3	0.00	0.00
FeO	8.24	17.03
MnO	0.18	0.99
MgO	14.85	25.68
CaO	21.08	1.13
Na_2O	0.27	0.02
Total	98.42	98.73
Cations per 6 Oxygens		
Si	1.889	1.964
Ti	0.022	0.004
Al	0.140	0.029
Cr	0.000	0.000
Fe^{+2}	0.261	0.527
Mn	0.006	0.031
Mg	0.838	1.416
Ca	0.855	0.045
Na	0.020	0.001
Sum	4.029	4.018
Wo	0.438	0.023
En	0.429	0.712
Fs	0.134	0.265

TABLE 4

PLAGIOCLASE ANALYSIS

Sample #	TJ-93	TJ-84	TJ-153	TJ-153	TJ-153	TJ-55	TJ-55
Comment	CPX	Core	Lrg XL	Same XL	Euhedral	Core	Core
Wt% Oxides							
SiO_2	56.43	58.00	58.86	59.42	57.42	57.61	57.71
TiO_2	0.03	0.01	0.03	0.02	0.02	0.03	0.03
Al_2O_3	26.85	27.06	25.64	24.88	26.08	26.63	26.27
BaO	0.00	0.00	0.00	0.00	0.00	0.00	0.00
Fe_2O_3	0.58	0.51	0.39	0.47	0.50	0.37	0.42
MgO	0.04	0.04	0.03	0.03	0.04	0.02	0.03
CaO	9.60	9.18	8.41	7.53	8.98	9.21	9.06
Na_2O	4.93	2.94	3.93	5.17	4.70	4.74	4.71
K_2O	1.04	0.88	0.94	1.30	0.77	0.89	0.94
Total	99.50	98.62	98.23	98.82	98.51	99.50	99.17
Cations per 8 Oxygens							
Si	2.553	2.610	2.660	2.680	2.606	2.592	2.604
Ti	0.001	0.000	0.001	0.001	0.001	0.001	0.001
Al	1.432	1.436	1.366	1.323	1.395	1.412	1.397
Ba	0.000	0.000	0.000	0.000	0.000	0.000	0.000
Fe^{+3}	0.020	0.017	0.013	0.016	0.017	0.012	0.014
Mg	0.003	0.003	0.002	0.002	0.003	0.001	0.002
Ca	0.465	0.443	0.407	0.364	0.437	0.444	0.438
Na	0.432	0.257	0.344	0.452	0.414	0.413	0.412
K	0.060	0.051	0.054	0.075	0.045	0.051	0.054
Sum	4.966	4.816	4.848	4.913	4.916	4.927	4.922
An	48.58	59.04	50.54	40.85	48.80	48.87	48.44
Ab	45.15	34.22	42.73	50.75	46.22	45.51	45.57
Or	6.27	6.74	6.73	8.40	4.98	5.62	5.99

PLAGIOCLASE ANALYSIS

Sample #	TJ-64	TJ-92A	TJ-93	TJ-93
Comment	Core	Lrg XL	Core Lrg	
Wt% Oxides				
SiO_2	56.20	56.74	56.04	56.59
TiO_2	0.02	0.00	0.04	0.01
Al_2O_3	26.38	26.28	26.95	26.58
BaO	0.00	0.00	0.00	0.00
Fe_2O_3	0.53	0.41	0.44	0.56
MgO	0.03	0.04	0.03	0.03
CaO	9.31	8.90	9.57	9.39
Na_2O	4.57	5.11	4.88	4.98
K_2O	0.98	1.11	0.89	0.93
Total	98.02	98.59	98.84	99.07
Cations per 8 Oxygens				
Si	2.573	2.584	2.549	2.567
Ti	0.001	0.000	0.001	0.000
Al	1.424	1.411	1.445	1.421
Ba	0.000	0.000	0.000	0.000
Fe^{+3}	0.018	0.014	0.015	0.019
Mg	0.002	0.003	0.002	0.002
Ca	0.457	0.434	0.466	0.456
Na	0.406	0.451	0.430	0.438
K	0.057	0.064	0.052	0.054
Sum	4.937	4.961	4.961	4.958
An	49.66	45.71	49.18	48.13
Ab	44.11	47.50	45.38	46.19
Or	6.23	6.79	5.45	5.68

TABLE 5

AMPHIBOLE ANALYSES

Sample #	TJ-164	TJ-164	TJ-164	TJ-164	TJ-164	TJ-153	TJ-153
Comment	Core of	Same as	Core	Core	Small	AMP	Small
Wt% Oxides	Lrg Crystal	above					
SiO_2	40.96	41.48	41.01	40.95	41.49	40.86	41.46
TiO_2	2.64	2.55	2.64	2.70	2.87	3.07	2.69
Al_2O_3	12.45	12.61	12.81	13.08	12.43	12.27	12.17
FeO	10.99	11.45	11.07	11.02	11.29	10.66	11.52
MnO	0.19	0.15	0.09	0.14	0.16	0.10	0.20
MgO	14.17	14.31	14.39	14.12	14.39	14.26	14.06
CaO	11.80	11.67	11.78	11.78	11.76	11.59	11.35
Na_2O	1.85	1.90	1.90	1.89	1.88	1.91	1.87
K_2O	1.35	1.29	1.32	1.30	1.30	1.41	1.26
Total	96.40	97.41	97.01	96.98	97.57	96.13	96.58
Total cations = 13 Exclusive of K, Na, Ca*							
Si	6.130	6.143	6.095	6.086	6.134	6.124	6.190
Ti	0.297	0.284	0.295	0.301	0.319	0.346	0.302
Al	2.196	2.202	2.245	2.292	2.166	2.168	2.142
Fe	1.378	1.421	1.379	1.372	1.399	1.339	1.441
Mn	0.025	0.019	0.012	0.018	0.021	0.013	0.026
Mg	3.160	3.158	3.187	3.127	3.171	3.185	3.129
Ca	1.892	1.852	1.876	1.876	1.863	1.861	1.816
Na	0.537	0.546	0.548	0.545	0.539	0.555	0.541
K	0.258	0.244	0.250	0.246	0.245	0.270	0.240
Sum	15.873	15.867	15.886	15.863	15.856	15.859	15.827

AMPHIBOLE ANALYSES

Sample #	TJ-153	TJ-153
Comment	Small XL	AMP
Wt% Oxides		
SiO_2	41.19	41.29
TiO_2	2.53	2.86
Al_2O_3	12.67	12.54
FeO	12.42	11.44
MnO	0.11	0.14
MgO	13.46	13.97
CaO	11.24	11.45
Na_2O	1.89	1.90
K_2O	1.15	1.21
Total	96.66	96.80
Total cations = 13 Exclusive of K, Na, Ca*		
Si	6.161	6.148
Ti	0.284	0.320
Al	2.234	2.201
Fe	1.557	1.428
Mn	0.014	0.018
Mg	3.001	3.100
Ca	1.801	1.827
Na	0.548	0.549
K	0.219	0.230
Sum	15.821	15.820

JDK

TABLE 6

BIOTITE ANALYSES

Sample #	TJ-93C	TJ-93C	TJ-93C	TJ-92A	TJ-92A	TJ-92A
SiO_2	36.57	36.14	37.93	36.36	36.95	35.73
Al_2O_3	14.00	14.40	13.93	14.33	14.64	14.55
TiO_2	5.35	5.52	5.34	6.23	7.12	7.13
Fe_2O_3	2.19	2.08	2.09	1.60	1.54	1.65
FeO	11.18	10.64	10.67	8.19	7.84	8.43
MnO	0.10	0.17	0.12	0.04	0.05	0.04
MgO	15.50	15.61	14.95	17.23	17.13	16.31
CaO	-	-	<0.01	<0.02	-	-
BaO	0.80	0.80	0.80	0.80	0.80	0.80
Na_2O	0.63	0.60	0.55	0.40	0.46	0.47
K_2O	8.92	9.11	8.91	9.54	9.48	9.28
Cl	-	-	-	-	-	-
F	-	-	-	-	-	-
H_2O	2.75	2.73	2.39	2.66	2.49	2.44
Sum	97.99	97.80	97.69	97.40	98.50	96.91
O=F, Cl	0.00	0.00	0.00	0.00	0.00	0.00
Total	97.99	97.80	97.69	97.40	98.50	96.91
Si	5.608	5.550	5.818	5.550	5.570	5.503
Al(IV)	2.392	2.450	2.182	2.450	2.430	2.497
Al(VI)	0.141	0.160	0.340	0.131	0.174	0.148
Ti(IV+VI)	0.617	0.638	0.616	0.715	0.807	0.826
Fe(+3)	0.253	0.240	0.241	0.184	0.175	0.191
Fe(+2)	1.434	1.367	1.369	1.046	0.989	1.086
Mn	0.013	0.022	0.016	0.005	0.006	0.005
Mg	3.542	3.573	3.418	3.920	3.849	3.744
Ca	0.000	0.000	0.002	0.003	0.000	0.013
Ba	0.048	0.048	0.048	0.048	0.047	0.048
Na	0.187	0.179	0.164	0.118	0.134	0.140
K	1.745	1.785	1.743	1.857	1.823	1.823
Cl	0.000	0.000	0.000	0.000	0.000	0.000
F	0.000	0.000	0.000	0.000	0.000	0.000
OH(calc)	2.737	2.715	2.362	2.628	2.415	2.420
Oct. Cat.	6.000	6.000	6.000	6.000	6.000	6.000
Int. Cat.	1.980	2.011	1.957	2.027	2.005	2.025
Mg/(Mg+Fe*)	0.677	0.690	0.680	0.761	0.768	0.746
X(Mg)	0.590	0.596	0.570	0.653	0.641	0.624
x(Sid)	0.184	0.202	0.170	0.168	0.176	0.197
X(Ann)	0.226	0.203	0.260	0.178	0.182	0.179

TABLE 7
ESTIMATED FUGACITIES OF SULFUROUS GASES*

Intensive Parameters	Lower Latite Flows	More Reducing	Upper Latite Flows
log $f(O_2)$	-10.25	-11.25	-11.25
T^o C	918	918	918
P (kbar)	3	3	3
f (H_2O) (bars)	1000	1000	2000
log f (S_2)	-0.037	-1.2	-1.2
log f (SO_2)	1.8	.19	.19
log f (SO_3)	-3.9	-6.0	-6.0
log f (H_2)	.15	.65	.95
log f (H_2S)	1.5	1.4	1.7

*fugacities of sulfurous gases calculated according to the methods of Whitney, 1984

TABLE 8

$^{40}AR/^{39}AR$ ANALYTICAL DATA FOR INCREMENTAL HEATING EXPERIMENTS ON MINERALS FROM VOLCANIC UNITS IN THE EAST TINTIC MOUNTAINS, UTAH.

Release temp (°C)	$(^{40}Ar/^{39}Ar)^*$	$(^{36}Ar/^{39}Ar)^*$	$(^{37}Ar/^{39}Ar)^c$	^{39}Ar % of total	$\%^{40}Ar$ non-atmos.$^+$	$^{36}Ar_{Ca}$ %	Apparent Age (Ma)**
Biotite							
Sample TJ-8-87: J = 0.006315							
475	7.75	0.02444	0.021	0.48	6.32	0.02	5.6 ± 9.3
610	18.09	0.04679	0.149	0.27	23.44	0.09	47.7 ± 16.1
645	8.76	0.01818	0.079	0.76	38.36	0.12	37.9 ± 4.2
680	5.62	0.00721	0.014	1.94	61.41	0.06	38.9 ± 1.6
715	4.09	0.00252	0.007	6.53	80.87	0.08	37.2 ± 0.7
750	3.64	0.00140	0.005	13.03	87.58	0.10	36.0 ± 0.2
775	3.64	0.00087	0.006	11.68	91.89	0.19	37.7 ± 0.3
800	3.59	0.00103	0.005	13.41	90.48	0.14	36.7 ± 0.2
825	3.61	0.00074	0.003	17.70	92.92	0.11	37.8 ± 0.3
850	3.70	0.00084	0.004	18.93	92.23	0.15	38.4 ± 0.3
Fusion	4.03	0.00105	0.011	15.27	91.40	0.29	41.5 ± 0.4
Total	3.86	0.00156	0.007	100.00	89.00	0.16	37.9 ± 0.4
Total without 475-680°C and fusion				81.28			37.4 ± 0.3
Sample TJ-112-88: J = 0.009245							
500	9.82	0.01669	0.283	0.74	49.95	0.46	80.0 ± 1.6
600	6.63	0.00703	0.132	1.27	68.72	0.51	74.4 ± 1.6
650	4.38	0.00448	0.039	2.04	69.69	0.24	50.2 ± 0.9
690	2.95	0.00209	0.017	7.11	78.92	0.22	38.4 ± 0.4
725	2.37	0.00065	0.013	10.18	91.65	0.54	35.9 ± 0.1
750	2.22	0.00035	0.009	11.30	95.07	0.69	34.9 ± 0.2
775	2.19	0.00028	0.008	11.03	95.95	0.73	34.7 ± 0.1
800	2.20	0.00026	0.008	9.95	96.27	0.83	35.0 ± 0.2
825	2.29	0.00044	0.012	6.34	94.14	0.76	35.7 ± 0.2
960	2.46	0.00099	0.014	17.51	87.94	0.39	35.8 ± 0.1
Fusion	2.44	0.00105	0.030	22.54	87.13	0.78	35.2 ± 0.1
Total	2.54	0.00105	0.020	100.00	89.51	0.62	36.6 ± 0.2
Total without 500-690°C				88.84			35.3 ± 0.1

TABLE 8 (Continued)

Sample TJ-84-88: J = 0.009622

525	15.64	0.04150	0.369	0.62	21.76	0.24	58.1 ± 5.3
625	3.23	0.00433	0.084	1.27	60.36	0.53	33.5 ± 0.7
675	2.45	0.00140	0.047	2.25	83.09	0.91	35.0 ± 0.5
710	2.19	0.00056	0.021	5.75	92.20	1.02	34.6 ± 0.3
740	2.08	0.00031	0.010	9.32	95.34	0.89	34.1 ± 0.2
765	2.06	0.00021	0.007	10.43	96.66	0.90	34.2 ± 0.1
790	2.08	0.00029	0.007	10.62	95.60	0.62	34.1 ± 0.2
813	2.11	0.00044	0.007	9.88	93.52	0.41	33.9 ± 0.2
840	2.16	0.00055	0.007	8.95	92.27	0.33	34.3 ± 0.2
870	2.30	0.00096	0.008	10.24	87.47	0.22	34.6 ± 0.1
905	2.56	0.00176	0.010	8.26	79.50	0.16	35.0 ± 0.4
940	2.92	0.00291	0.017	6.75	70.39	0.16	35.3 ± 0.7
980	2.92	0.00291	0.023	8.67	70.37	0.22	35.3 ± 0.4
1020	2.79	0.00255	0.057	6.13	72.93	0.61	35.0 ± 0.5
Fusion	2.47	0.00245	0.478	0.87	71.92	5.30	30.5 ± 2.3
Total	2.44	0.00142	0.022	100.00	86.15	0.55	34.6 ± 0.4
Total without 525-625°C and fusion				97.24			34.5 ± 0.2

Sample HS-UTH-86-2: J = 0.009895

525	10.37	0.02782	0.104	2.47	20.72	0.10	37.9 ± 2.4
625	6.00	0.01315	0.028	7.75	35.23	0.06	37.4 ± 0.9
675	2.52	0.00202	0.012	11.44	76.07	0.16	33.9 ± 0.2
710	2.18	0.00090	0.010	11.30	87.53	0.30	33.7 ± 0.1
735	2.15	0.00077	0.012	7.11	89.20	0.42	33.9 ± 0.2
760	2.16	0.00098	0.012	5.38	86.37	0.33	33.1 ± 0.3
785	2.26	0.00115	0.012	4.68	84.71	0.29	33.8 ± 0.4
810	2.47	0.00181	0.019	3.87	78.08	0.28	34.0 ± 0.3
840	2.48	0.00179	0.022	4.69	78.52	0.33	34.4 ± 0.6
875	2.38	0.00144	0.022	5.90	82.00	0.42	34.6 ± 0.5
910	2.26	0.00124	0.021	8.81	83.53	0.45	33.4 ± 0.2
945	2.13	0.00083	0.019	14.69	88.22	0.62	33.2 ± 0.2
Fusion	2.09	0.00074	0.039	11.90	89.49	1.45	33.2 ± 0.3
Total	2.74	0.00276	0.022	100.00	79.30	0.48	34.0 ± 0.4
Total without 525, 625, 945°C and fusion				89.78			33.6 ± 0.2

TABLE 8 (Continued)

Muscovite

Sample KS-2A-87: J = 0.006345

450	4.25	0.00291	0.013	11.72	78.89	0.13	38.0 ± 0.4
475	3.57	0.00094	0.012	14.30	91.19	0.38	36.9 ± 0.5
500	3.70	0.00136	0.013	12.27	88.13	0.41	37.0 ± 0.3
525	3.49	0.00066	0.012	16.86	93.37	0.54	36.9 ± 0.5
550	3.47	0.00070	0.012	15.99	92.99	0.50	36.6 ± 0.3
575	3.52	0.00085	0.011	5.70	91.82	0.50	36.6 ± 0.5
600	3.45	0.00099	0.010	6.31	90.48	0.30	35.4 ± 1.2
625	3.71	0.00202	0.010	5.72	82.89	0.14	34.8 ± 0.5
660	3.72	0.00175	0.017	3.68	85.08	0.27	35.9 ± 0.8
695	3.73	0.00233	0.014	2.35	80.53	0.18	34.0 ± 1.8
740	3.90	0.00350	0.012	1.46	72.49	0.10	32.1 ± 3.2
800	4.18	0.00494	0.041	1.10	64.28	0.24	30.5 ± 4.3
Fusion	4.85	0.00442	0.081	2.55	72.41	0.53	39.8 ± 1.2
Total	3.69	0.00143	0.016	100.00	88.02	0.38	36.5 ± 0.6
Total without 695°C-Fusion				92.54			36.7 ± 0.5

Sanidine

Sample TJ-77-88: J = 0.010020

700	2.76	0.00262	0.112	9.99	72.04	1.16	35.6 ± 0.4
800	1.95	0.00017	0.052	17.29	97.36	8.46	33.9 ± 0.1
850	1.94	0.00013	0.040	16.73	97.90	8.44	34.0 ± 0.1
890	1.95	0.00012	0.034	19.36	97.95	7.48	34.1 ± 0.1
930	1.96	0.00016	0.031	10.25	97.38	5.24	34.2 ± 0.2
970	1.99	0.00026	0.029	13.19	95.92	3.02	34.2 ± 0.2
1020	2.09	0.00054	0.030	10.16	92.22	1.51	34.5 ± 0.2
1100	2.47	0.00188	0.041	1.94	77.33	0.60	34.2 ± 1.0
Fusion	3.18	0.00474	0.058	1.08	55.94	0.33	31.9 ± 1.8
Total	2.07	0.00053	0.045	100.00	93.49	5.54	34.3 ± 0.2
Total without 700, 1100°C and fusion				86.99			34.1 ± 0.1

[a] Measured.

[b] Corrected for post-irradiation decay of ^{37}Ar (35.1 day 1/2-life).

[c] $[^{40}Ar_{tot.} - (^{36}Ar_{atmos.})\ (295.5)] \ / \ ^{40}Ar_{tot.}$.

[d] Calculated using correction factors of Dalrymple et al. (1981); two sigma, intralaboratory errors.

TABLE 9
$^{36}AR/^{40}AR$ VS. $^{39}AR/^{40}AR$ ISOTOPE CORRELATIONS USING PLATEAU ANALYTICAL DATA FROM INCREMENTAL HEATING EXPERIMENTS ON MINERALS FROM VOLCANIC UNITS IN THE EAST TINTIC MOUNTAINS, UTAH.

Sample	Isotope Correlation Age (Ma)*	$^{40}Ar/^{36}Ar$ Intercept**	MSWD	% of Total ^{39}Ar	Calculated $^{40}Ar/^{39}Ar$ Plateau (Ma)***
		Biotite			
TJ-8-87	34.7 ± 0.2	326.8 ± 26.3	1.84	81.28	37.4 ± 0.3
TJ-112-88	34.7 ± 0.1	352.2 ± 33.1	1.58	88.84	35.3 ± 0.1
TJ-84-88	34.2 ± 0.1	322.6 ± 21.3	0.14	97.24	34.5 ± 0.2
HS-UTH-86-2	33.0 ± 0.2	323.2 ± 26.1	0.17	89.78	33.6 ± 0.2
		Muscovite			
KS-2A-87	36.6 ± 0.2	346.3 ± 31.3	0.19	92.54	36.7 ± 0.5
		Sanidine			
TJ-77-88	34.0 ± 0.1	360.3 ± 42.6	0.43	86.99	34.1 ± 0.1

* Calculated using the inverse abscissa intercept ($^{40}Ar/^{39}Ar$ ratio) in the age equation

** Inverse ordinate intercept.

*** Table 1.

FIGURE CAPTIONS

Figure 1. A. Ore deposits, monzonite stocks, inferred caldera of Morris (1975), and index map of the East Tintic Mountains (compiled from Morris, 1975; Morris and Morgensen, 1978). Replacement and vein ore deposits are shown as solid black; monzonite intrusions are stippled (sills of Morris (1975) are not shown); other features as labeled in figure. Part of the area mapped by Keith and Kim during the summer of 1988 is outlined and summarized in part B. The immediate vicinity of the sub-economic Cu-Mo deposit is covered by alluvium or unmapped (mapped by Hannah and Macbeth, in prep.). B. Map summarizing Plate 2 which shows the relationship between monzonite intrusions of Silver City lithology (in solid black), argillic-phyllic alteration and moderate to intensely silicified rock (stippled). In addition, biotite latite dikes (outlined only), some of which contain magmatic sulfides are also summarized from Plate 1.

Figure 2. The lower member of the Golden's Ranch Formation in Government Canyon. A. Finely-laminated shale at the face of a small adit near Jumpoff Spring. The gray color is imparted by finely disseminated pyrite which has oxidized to limonite along bedding planes and fractures. B. Sample of altered and oxidized shale that exhibits calcareous gastropod shells preferentially replaced by pyrite and subsequently oxidized to limonite.

Figure 3. The upper member of the Golden's Ranch Formation in Government Canyon. A. Outcrop of the lower portion of the upper member. The unit labeled "A" is the upper, reworked volcaniclastic material above the agglomerate. The "B" unit represents a sharp transition to organic-bearing, limonite-rich shale that was probably pyrite-rich prior to oxidation. The "C" unit contains abundant plant fossils and organic material (similar to "B"), but lacks limonite-stain. "D" is a thin layer of limestone. More shale and limestone (~1 m thick) occur above "D", but are not well exposed. B. Plant fossils present in the limonite-stained shale (from the outcrop illustrated in part A.).

Figure 4. Photomicrographs and X-ray maps of exsolved magmatic sulfides from a biotite latite dike (TJ-84) and a lava vitrophyre (TJ-55). A. This large magmatic sulfide bleb is composed mostly of pyrite (light yellow), interstial degassed pyrrhotite or "Fe-oxide" (gray), surrounded by a rim of exsolved chalcopyrite (orange). [All of the surrounding silicates and oxides are gray due to carbon coating which enhances the contrast in sulfide colors.] The maximum diameter of the entire grain is 450 microns. Preservation of unusually large magmatic sulfide blebs such as this one seems to be dependent upon occurring within a glomeroporphyritic clot of phenocrysts and glass. The bleb margin which extended out of the clot was apparently broken off (along the preferred exsoloution planes) during magma emplacement (note absent rim of chalcopyrite along the

bottom). B. This smaller equant exsolved sulfide bleb (45 microns in diameter) is hosted entirely within a clinopyroxene phenocryst, but exhibits many of the characteristics of the larger grain. Even this small grain is much larger than those generally preserved in calc-alkaline ash-flows such as the Bishop Tuff or Fish Canyon Tuff. C. These X-ray maps for Fe (upper) and S (lower) are inverted images of the area within the black square in part A. This pair of maps documents that the Fe distribution within the degassed sulfide is fairly homogenous as it would have been in the original iron mono-sulfide melt (MSS). The exception to this is the chalcopyrite rim (resulting from the early exsolved Cu-rich ISS). Consequently, the exsolution and degassing processes consist of migration of S. X-ray mapping for As shows a pattern similar to S. Continued degassing removes almost all of the S and As (and probably Ag, Au, and Cu). D. Comparison of two magmatic sulfide blebs locked within a single titanomagnetite grain (TJ-55). Abbreviations for phases illustrated are: chal=chalcopyrite, timag=titanomagnetite, magh= maghemite, py=pyrite, pyrr=pyrrhotite, and hem=hematite. As the margin of the titanomagnetite and the upper sulfide bleb react with the oxygen in the cooling lava vitrophyre, titanomagnetite oxidizes to become maghemite and the pyrrhotite oxidizes to pyrite and hematite (?). E. Magmatic sulfide bleb present in microcrystalline matrix which has been strongly oxidized,

degassed of H_2S, and resorbed (TJ-84). Note how little pyrite (white) remains within the grain after strong degassing; the chalcopyrite (orange) rim is mostly absent; but apparently is more resistant to degassing. Escaping H_2S may have reacted with the adjacent diopside phenocryst to create the mantling As-rich pyrite. F. Reflected light photomicrograph of an exsolved composite magmatic sulfide bleb present in a glomeroporphyritic clot from a biotite latite flow vitrophyre (TJ-55). This composite magmatic sulfide grain is 140 microns in length and consists mainly of three phases: chalcopyrite (orange), Ni-, Co-bearing pyrite (yellow), and a small degassed Fe-oxide core (gray). Barely apparent in this photo are small exsolved phases of cubanite (light yellow) in the chalcopyrite and Ni-rich zones (nearly white) in the pyrite. The grain is surrounded mostly by glass (brown). Distler et al. (1986) describe amazingly similar sulfide blebs present in oceanic basalts in which the sulfide bleb has segregated into two halves; one half is a Ni-bearing MSS and the other half is close to cubanite in composition. Lightfoot et al. (1984) note very similar magmatic sulfide globules in the Insizwa Cu-Ni deposit except the Cu-rich half is dominantly chalcopyrite as in this illustration. G. Secondary electron image of the same grain in part F with an inset backscatter electron image. The backscatter electron image contrasts the differences in average atomic weight of each phase; this enhances the contrast of the darker gray

degassed hematite core. Degassing of H_2S occurs along major fractures (or creates the fractures due to volume reduction).

Figure 5. [see caption on figure]

Figure 6. Microprobe analyses of clinopyroxenes. Analyses from Table 3 are plotted on the pyroxene quadrilateral. Those clinopyroxenes with orthopyroxene pairs show the two pyroxene temperature for that pair along the tie-line (thermometer of Wells, 1977; compositions recalculated according to the methods of Lindsley and Anderson, 1983). Solid circles and best-fit line through them shows the compositional variations and trend present in one sample (TJ-64).

Figure 7. $^{40}Ar/^{39}Ar$ age spectra of: A) biotite from sample TJ-8(-87); B) biotite from TJ-112(-88); C) biotite from sample TJ-84(-88); D) biotite from sample HS-UTH-86-2 (courtesy of J. Hannah); E) muscovite from sample KS-2A(-87); and F) sanidine from sample TJ-77(-88). Two-sigma intralaboratory uncertainties indicated by vertical width of bars. Experimental temperatures of argon evolution increase from left to right. Total gas and plateau ages (plateau increments outlined by arrows) listed on each spectrum.

Figure 1

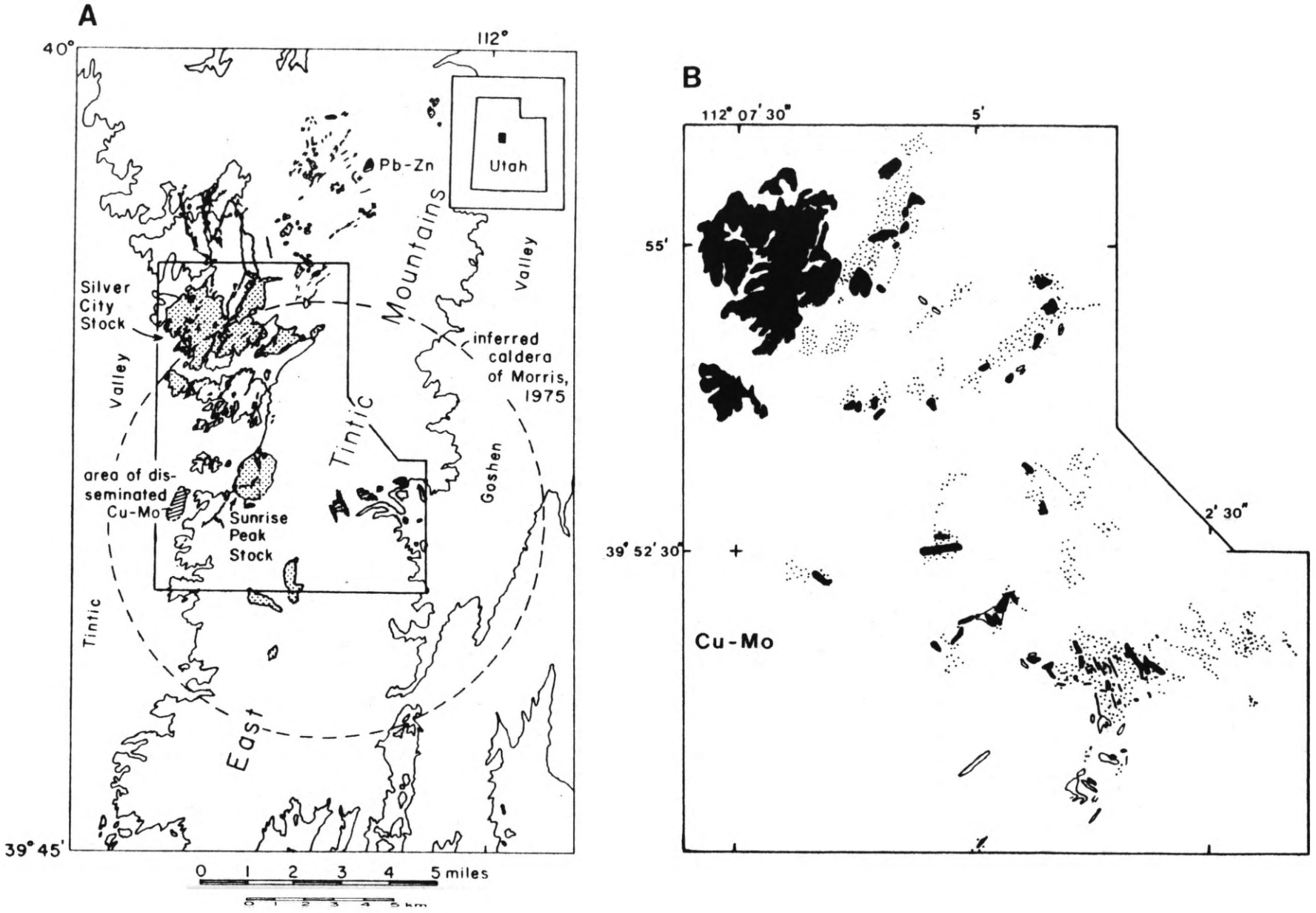
A
40°
112°
Utah
Pb-Zn
Silver City Stock
Tintic Mountains
Valley
inferred caldera of Morris, 1975
Valley
area of disseminated Cu-Mo
Sunrise Peak Stock
Tintic
Goshen
East
39°45'
0 1 2 3 4 5 miles
B
112° 07' 30"
5'
55'
2' 30"
39° 52' 30"
Cu-Mo

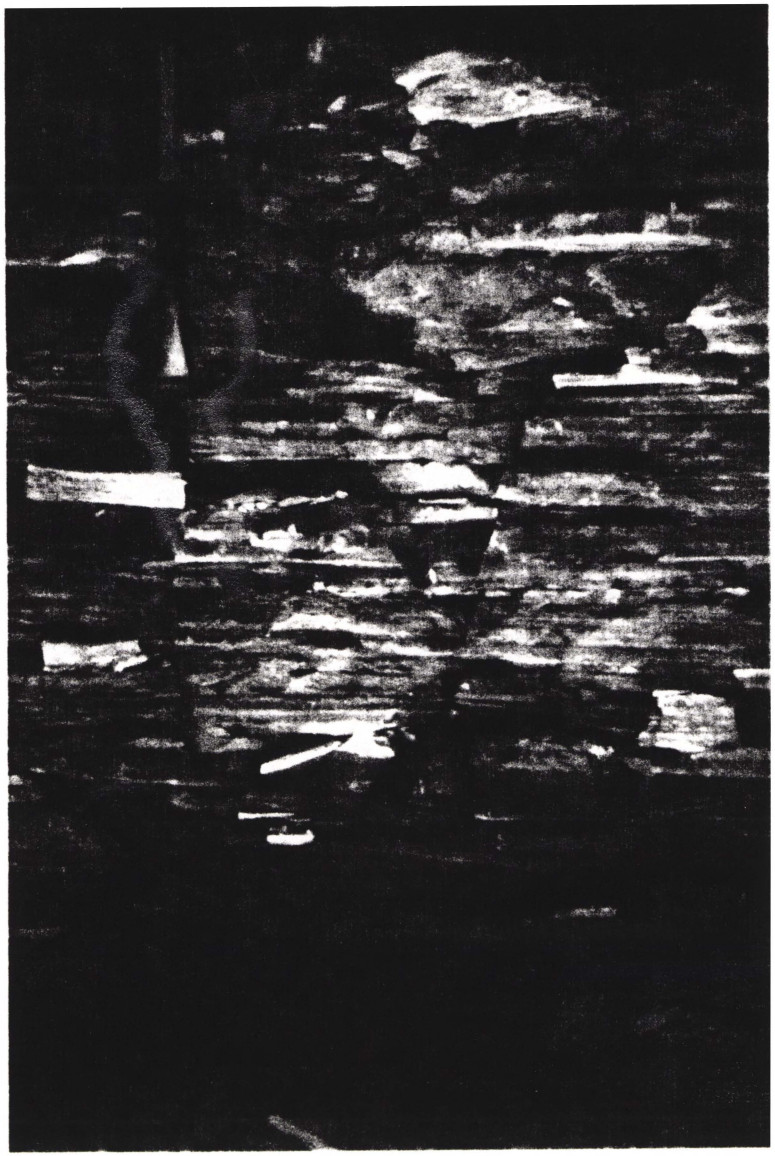

A

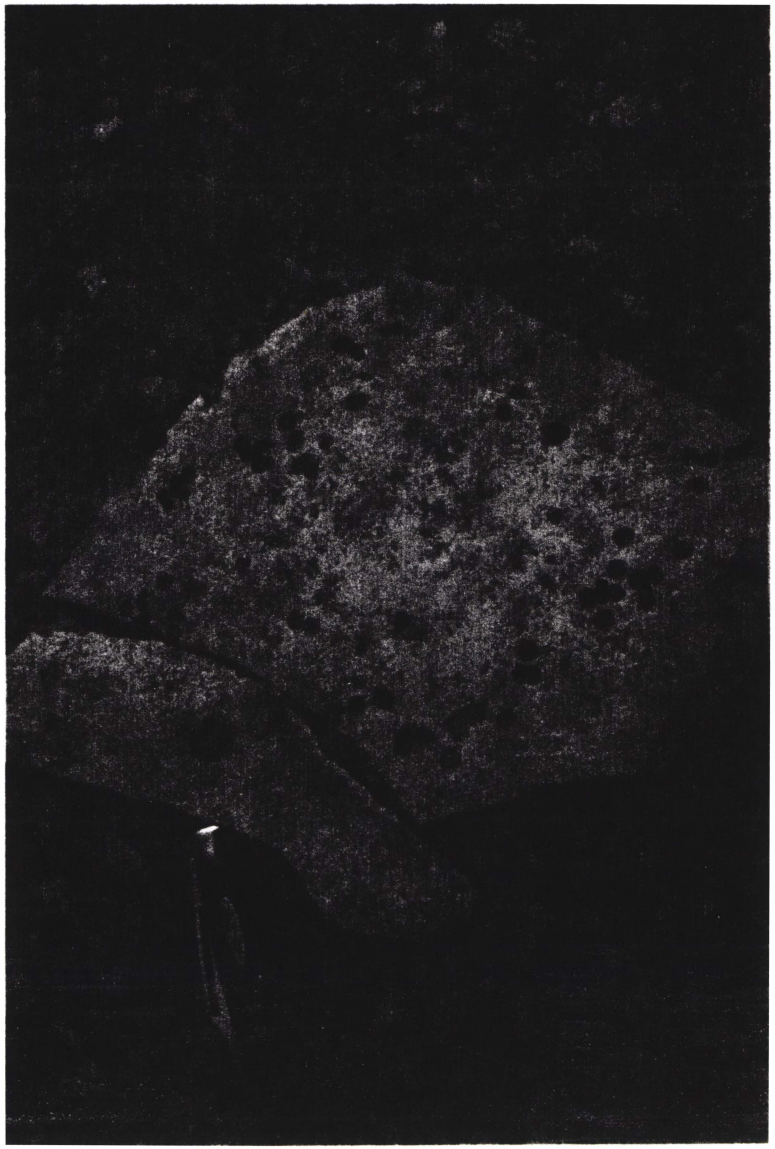

B

color copy for sale in bookstore

Figure #2

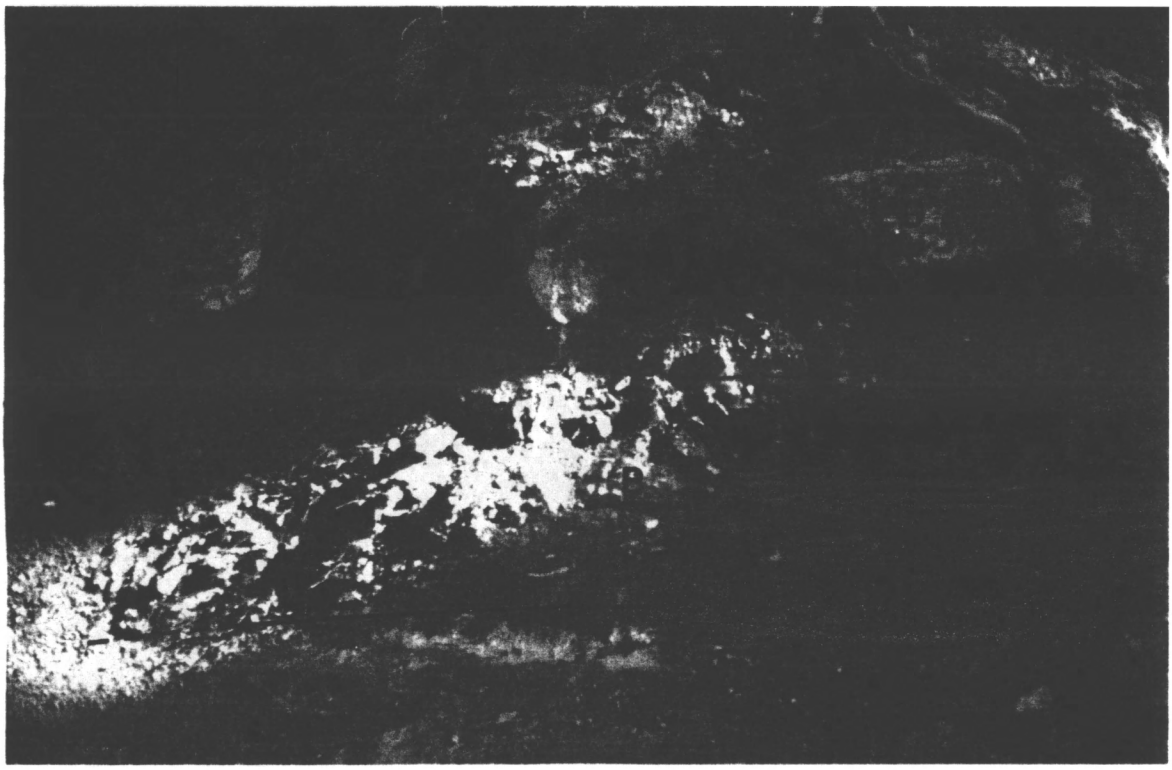

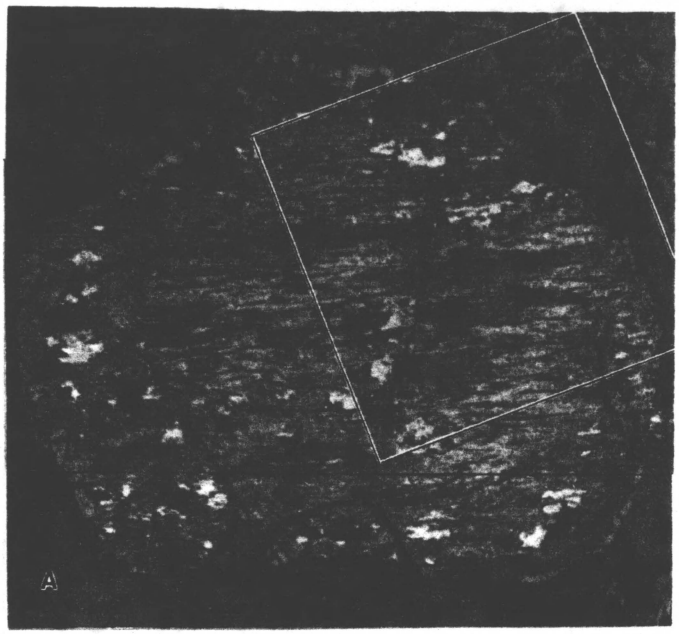

C.

X-ray Map for Fe

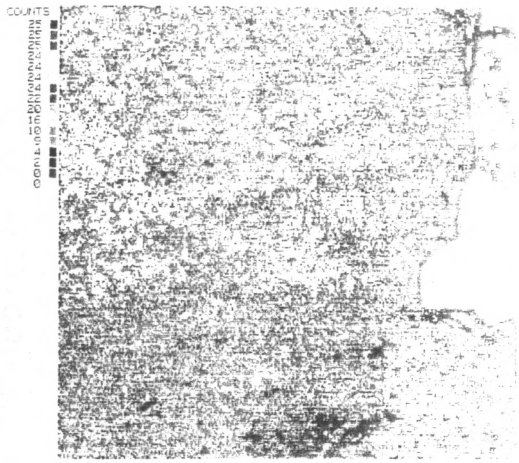

X-ray Map for S

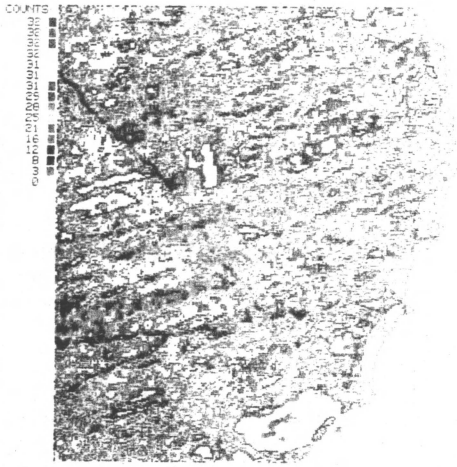

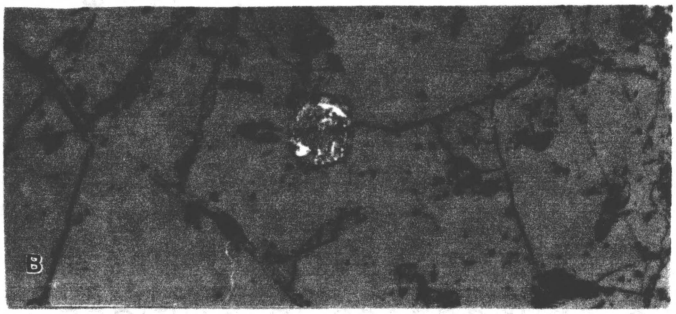

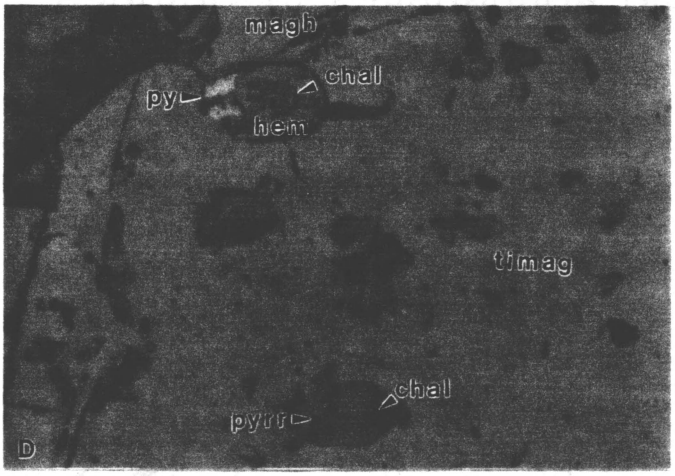

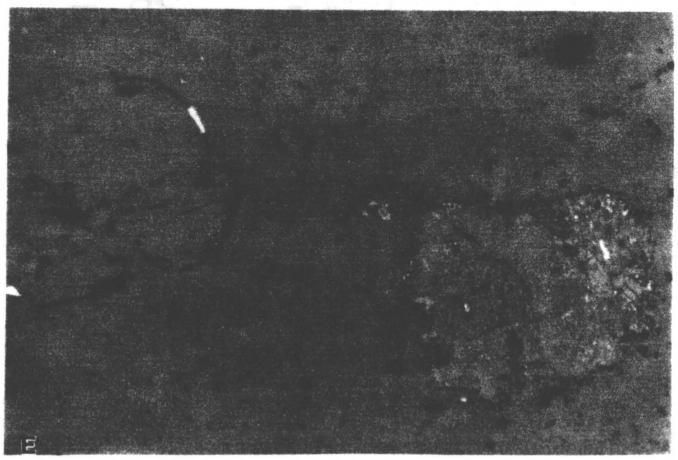

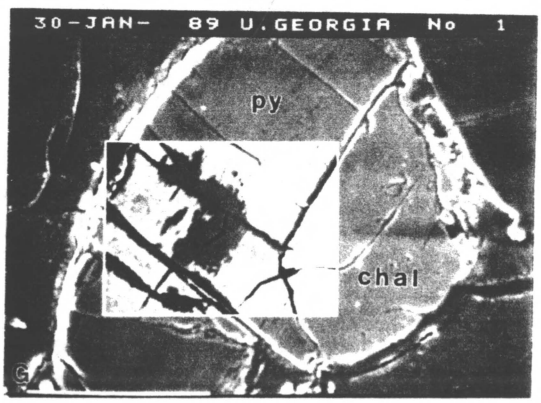

Figure 4

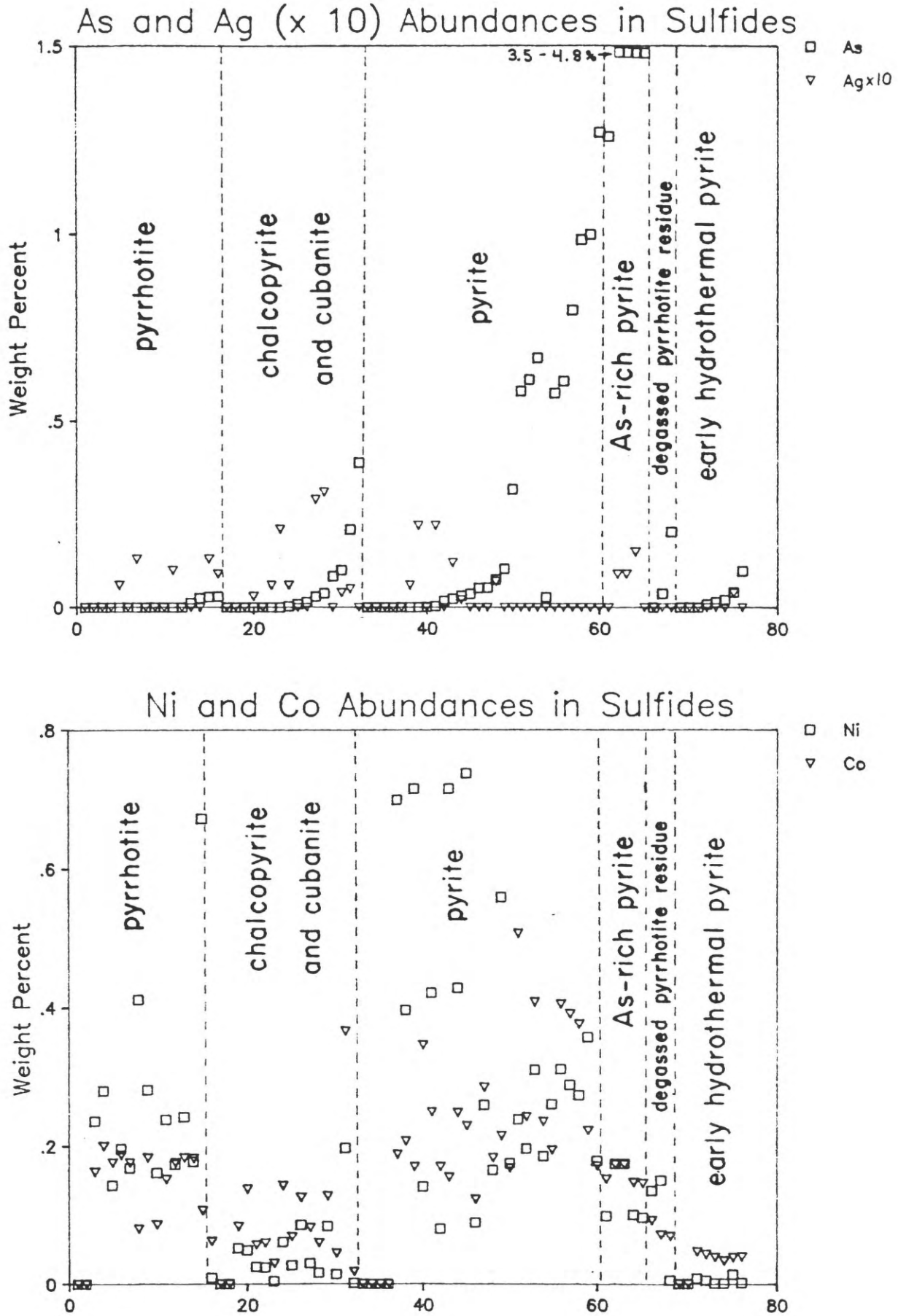

Figure 3.5. Minor element content of sulfides plotted versus different sulfide occurrences. A. As and Ag(x 10) abundances. B. Ni and Co abundances.

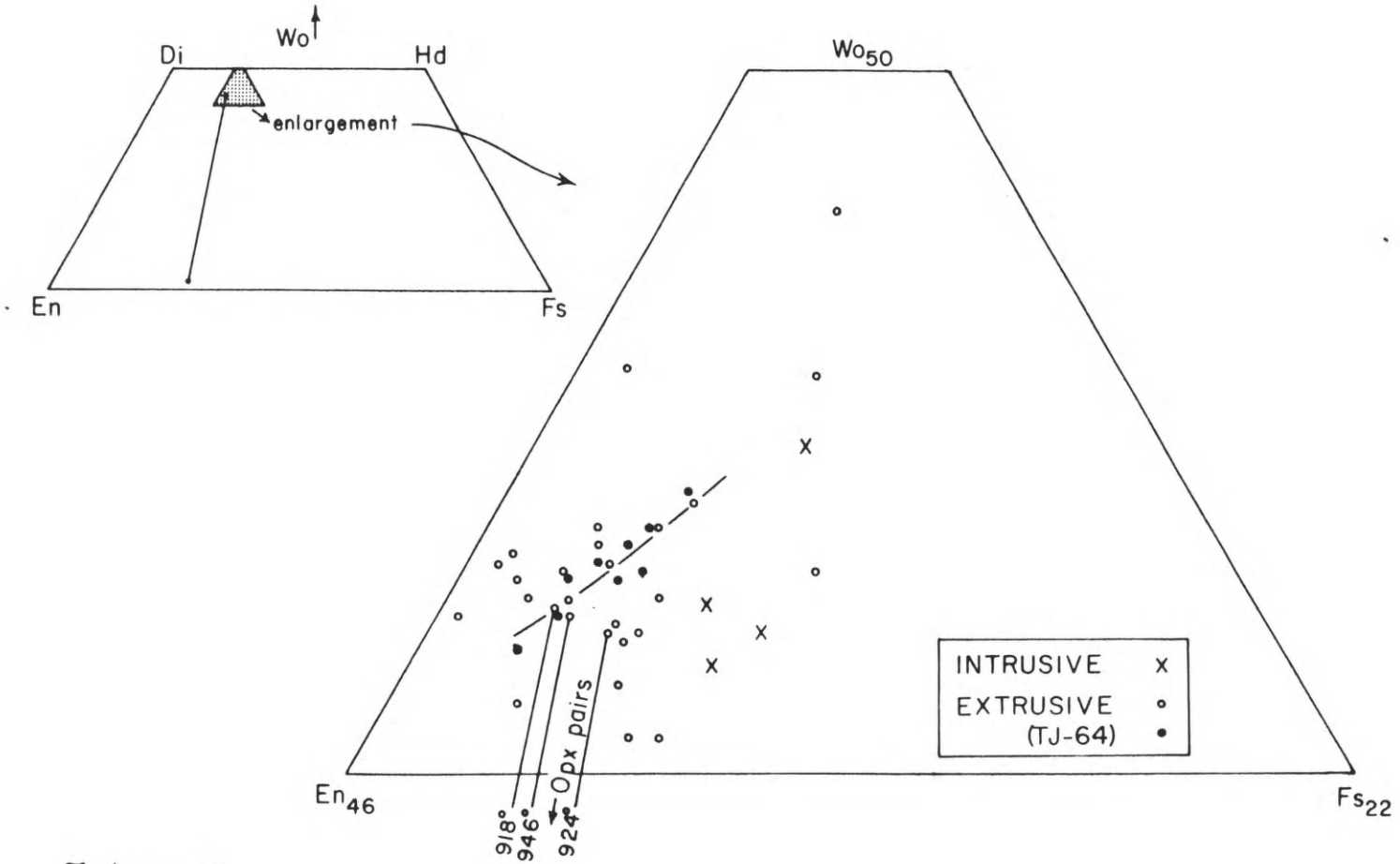
Wo
Di
Hd
enlargement
En
Fs
Wo50
En46
Fs22
INTRUSIVE
EXTRUSIVE
(TJ-64)
Opx pairs
918°
946°
924°

Figure 6

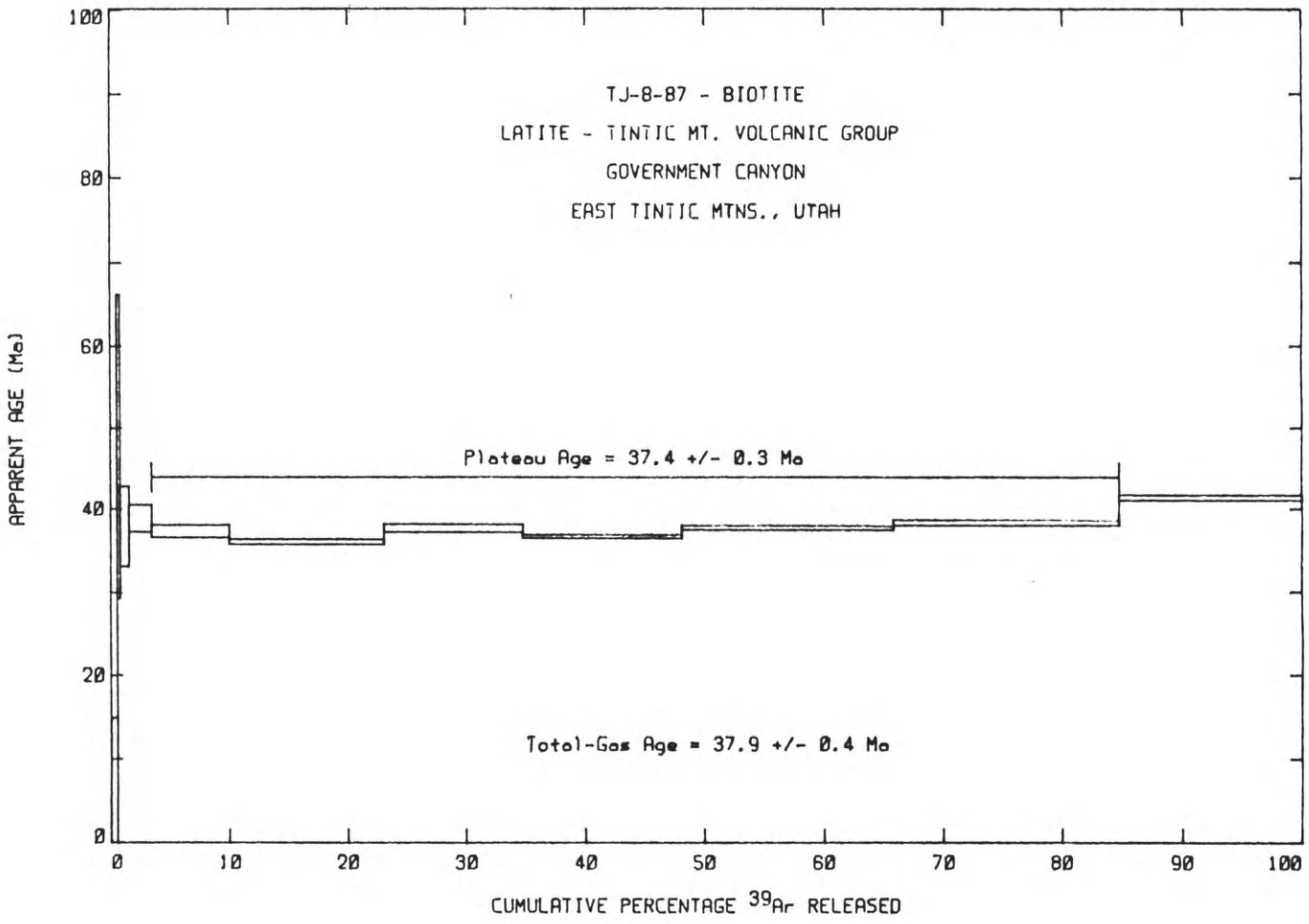
TJ-8-87 - BIOTITE
LATITE - TINTIC MT. VOLCANIC GROUP
GOVERNMENT CANYON
EAST TINTIC MTNS., UTAH
Plateau Age = 37.4 +/- 0.3 Ma
Total-Gas Age = 37.9 +/- 0.4 Ma
APPARENT AGE (Ma)
CUMULATIVE PERCENTAGE 39Ar RELEASED
0
20
40
60
80
100
0
10
20
30
40
50
60
70
80
90
100

Figure 7A

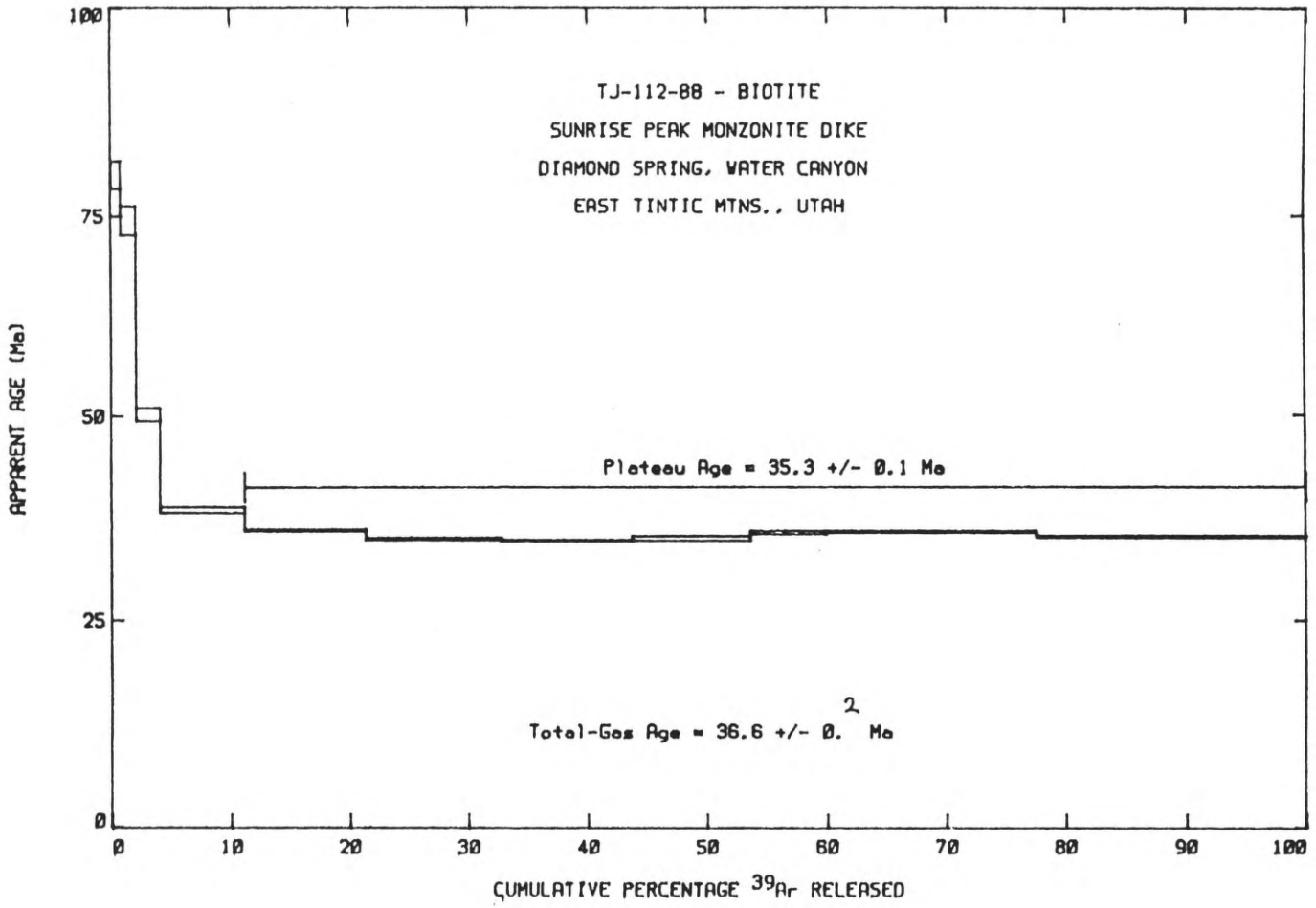
TJ-112-88 - BIOTITE
SUNRISE PEAK MONZONITE DIKE
DIAMOND SPRING, WATER CANYON
EAST TINTIC MTNS., UTAH
Plateau Age = 35.3 +/- 0.1 Ma
Total-Gas Age = 36.6 +/- 0.2 Ma
APPARENT AGE (Ma)
100
75
50
25
0
0
10
20
30
40
50
60
70
80
90
100
CUMULATIVE PERCENTAGE 39Ar RELEASED

Figure 7B

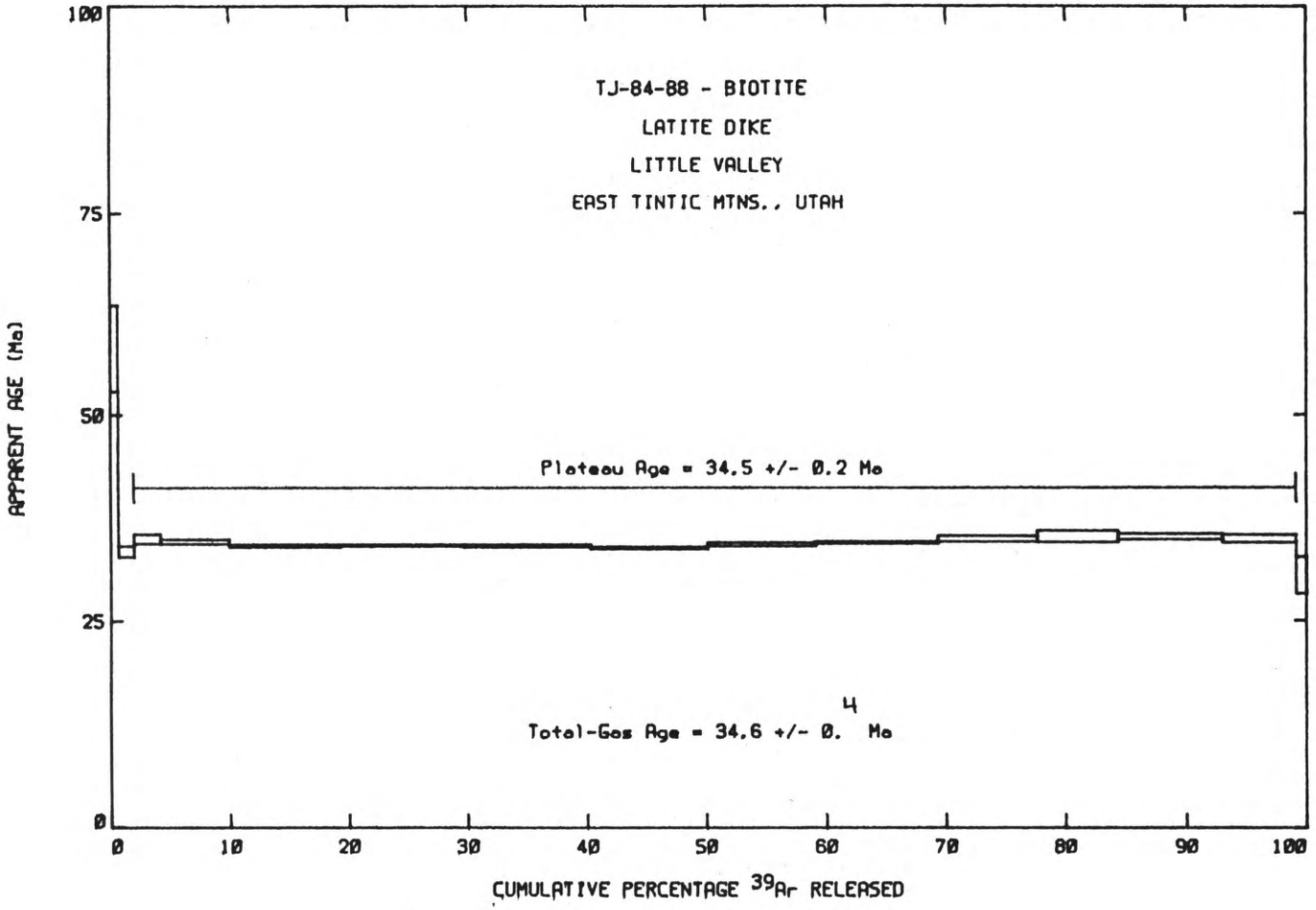
TJ-84-88 - BIOTITE
LATITE DIKE
LITTLE VALLEY
EAST TINTIC MTNS., UTAH
Plateau Age = 34.5 +/- 0.2 Ma
Total-Gas Age = 34.6 +/- 0.4 Ma
APPARENT AGE (Ma)
CUMULATIVE PERCENTAGE 39Ar RELEASED
100
75
50
25
0
0
10
20
30
40
50
60
70
80
90
100

Figure 7C

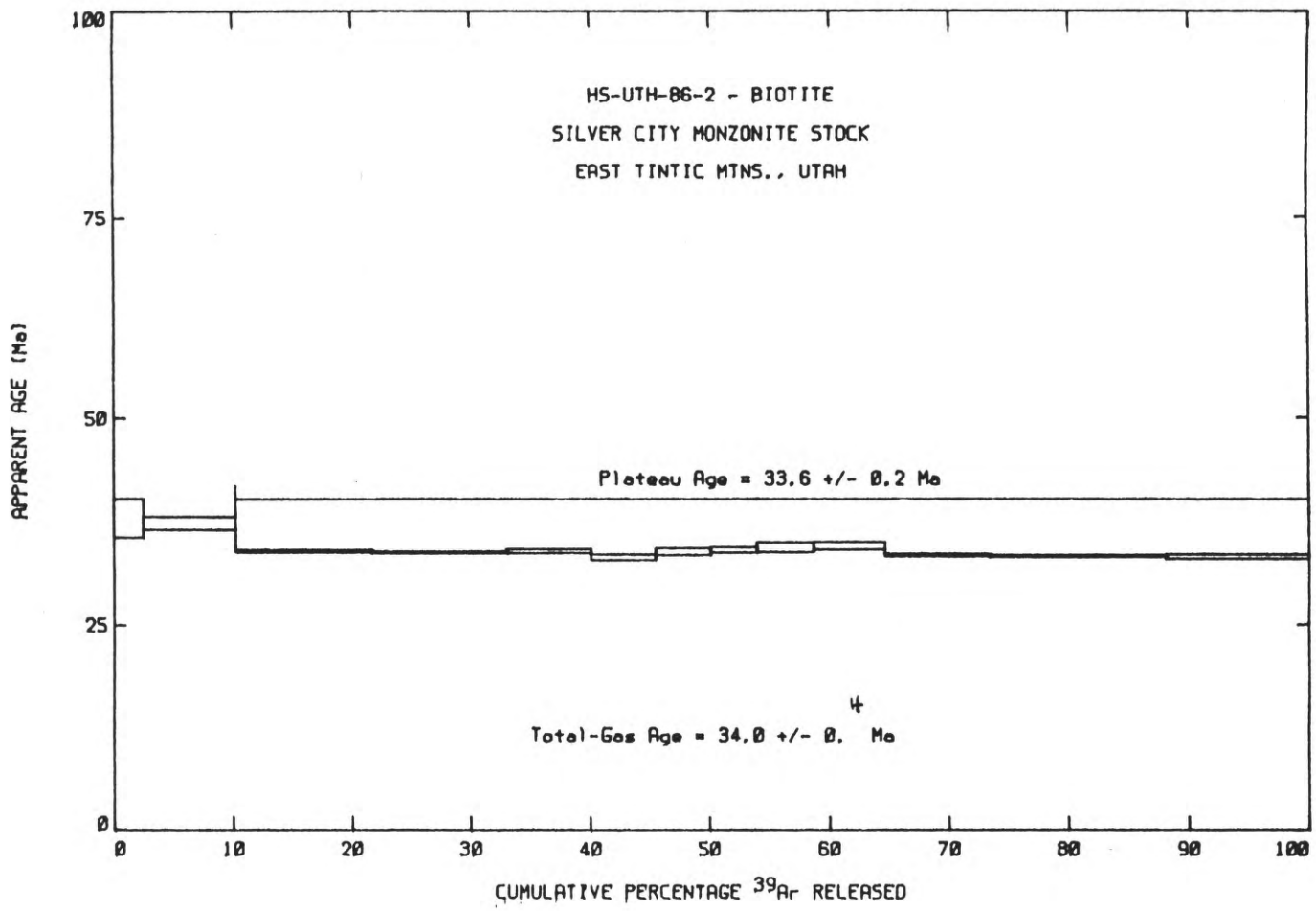
HS-UTH-86-2 - BIOTITE
SILVER CITY MONZONITE STOCK
EAST TINTIC MTNS., UTAH
Plateau Age = 33.6 +/- 0.2 Ma
Total-Gas Age = 34.0 +/- 0. Ma
APPARENT AGE (Ma)
100
75
50
25
0
0
10
20
30
40
50
60
70
80
90
100
CUMULATIVE PERCENTAGE 39Ar RELEASED

Figure 7D

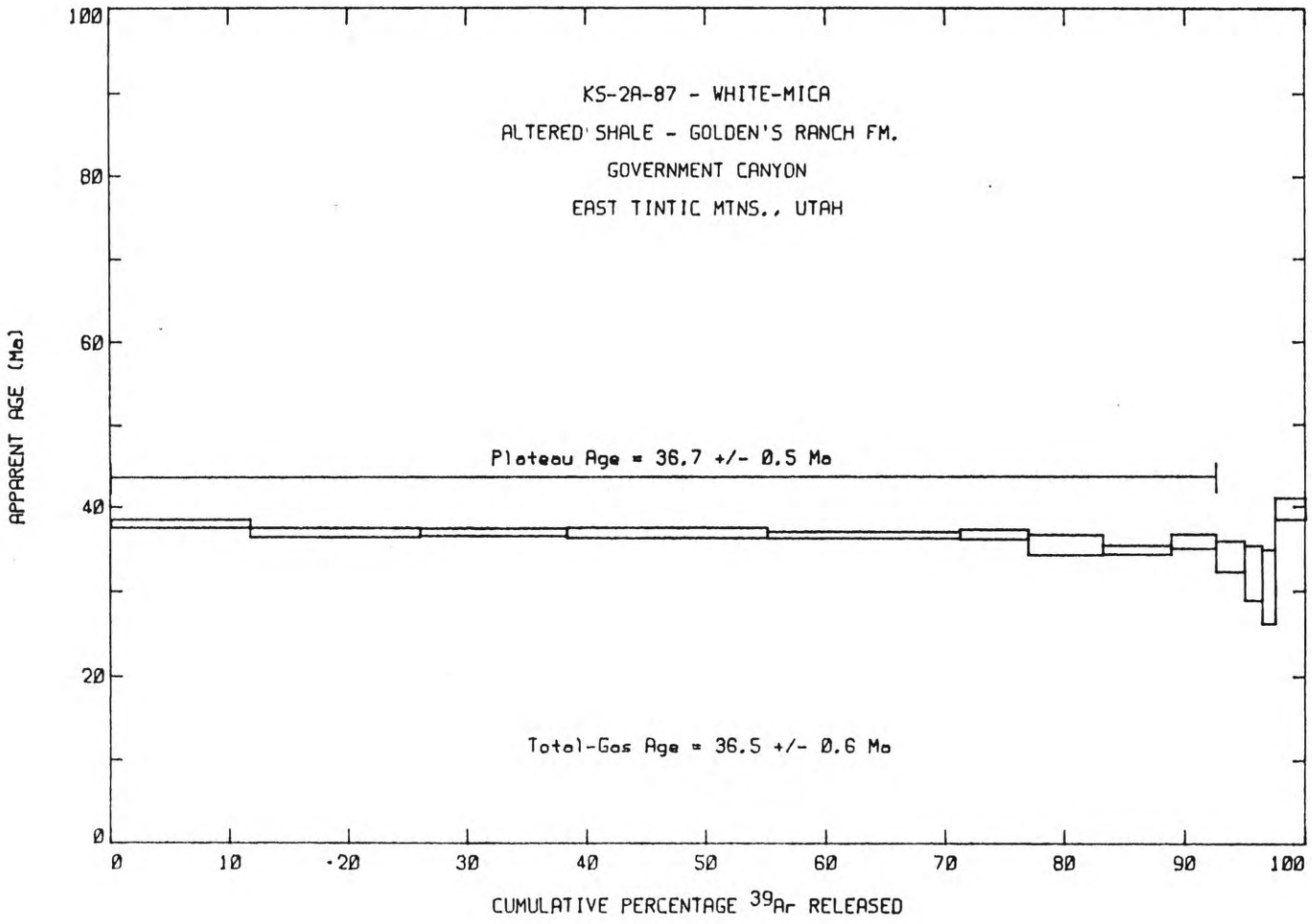
KS-2A-87 - WHITE-MICA
ALTERED SHALE - GOLDEN'S RANCH FM.
GOVERNMENT CANYON
EAST TINTIC MTNS., UTAH
Plateau Age = 36.7 +/- 0.5 Ma
Total-Gas Age = 36.5 +/- 0.6 Ma
APPARENT AGE (Ma)
CUMULATIVE PERCENTAGE 39Ar RELEASED
100
80
60
40
20
0
0
10
20
30
40
50
60
70
80
90
100

Figure 7E

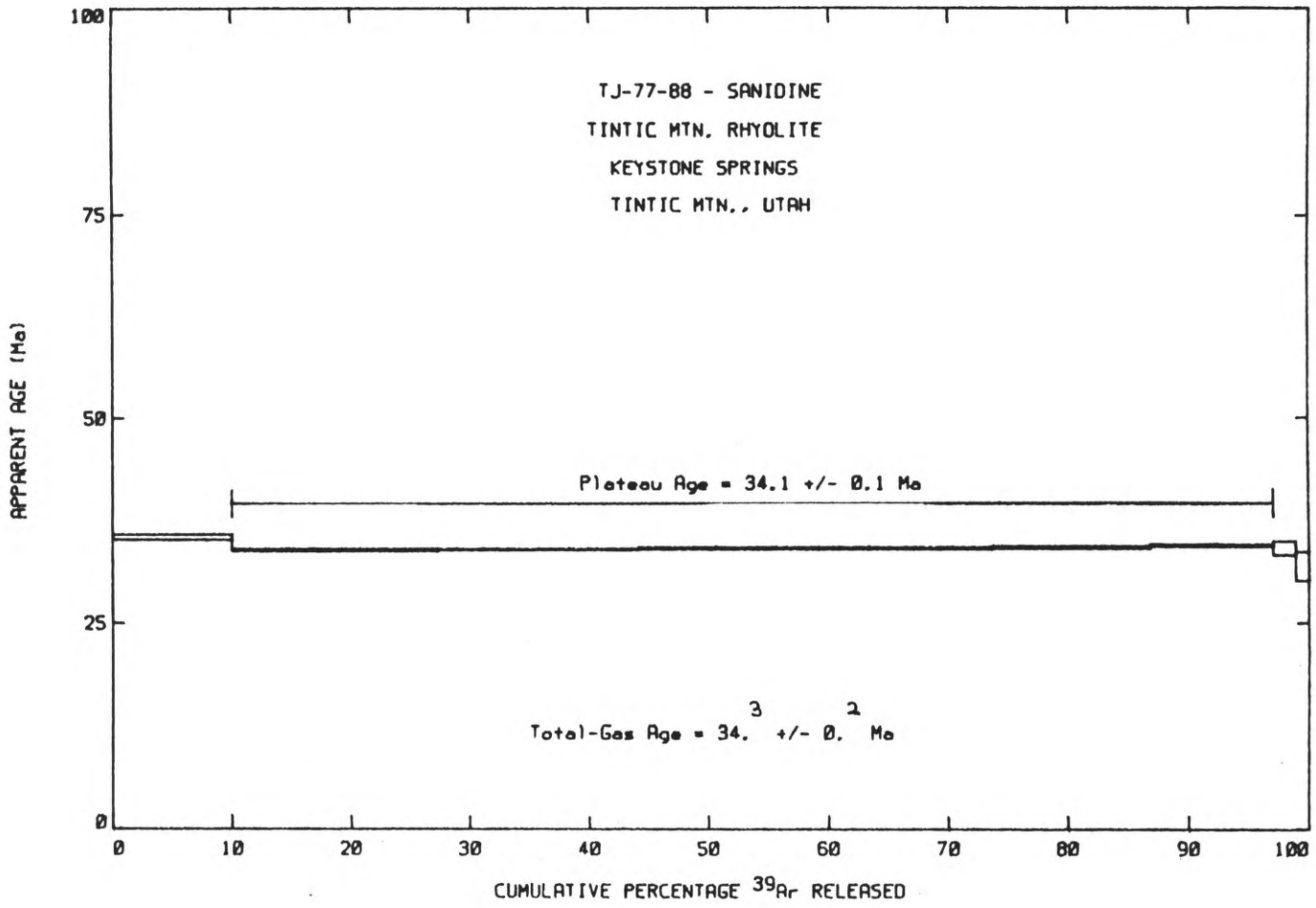
TJ-77-88 - SANIDINE
TINTIC MTN. RHYOLITE
KEYSTONE SPRINGS
TINTIC MTN., UTAH
Plateau Age = 34.1 +/- 0.1 Ma
Total-Gas Age = 34.3 +/- 0.2 Ma
APPARENT AGE (Ma)
CUMULATIVE PERCENTAGE 39Ar RELEASED
100
75
50
25
0
0
10
20
30
40
50
60
70
80
90
100

Figure 7F

APPENDIX 1: SAMPLE DESCRIPTIONS AND LOCATIONS

TJ-8; biotite latite vitrophyre; 39° 50′ 56" N, 112° 03′ 25" W

Clinopyroxene, plagioclase, biotite, and oxidized titanomagnetite in a glassy matrix. In reflected light it can be noted that ~95% of the titanomagnetite grains are oxidized to maghemite and pyrrhotite is exceedingly rare. Perhaps only 12 spherical grains in the larger section and all but 1 are 10 microns or less in size and present in titanomagnetite. Most of the of the sulfide may have degassed, but I suspect it was never very sulfide-rich.

TJ-18; 39° 50′ 53" N, 112° 04′ 01" W

Mafic flow unit. Black, dense, porphyritic basalt flow. In thin section, plagioclase feldspar, augite, and minor olivine constitutes the phenocryst phases, showing glomerophyric texture. Most of the ferromagnesian minerals are slightly altered. The groundmass is holocrystalline and consists of plagioclase laths and minute grains of augite and titanomagnetite.

TJ-51; lower biotite latite flow; 39° 52′ 00" N, 112° 03′ 11" W

Plagioclase, biotite, clinopyroxene, and titanomagnetite and apatite phenocrysts set in fine-grained matrix. Flow foliation is strong with stronger oxidation effects along flow-parallel fractures. Thick oxidation halos around biotite margins. Traces of chlorite, calcite, and hematite may relict former hornblende (uncertain). Plagioclase is mostly free of alteration, and numerous melt or crystal inclusions. Some included titanomagnetite in the cpx.

TJ-55; vitrophyre of biotite latite flow; 39° 52′ 56" N, 112° 03′ 10" W

Plagioclase, biotite, clinopyroxene, titanomagnetite, and apatite pheno-

crysts set in a black glassy matrix. Most, matrix has transparent microlites. Amber glass with no microlites is present within voids in large glomeroporphyritic clots. No clay, chlorite, sericite, or oxidation of biotite. A few symplectic oxide (spinels) in cpx. Plagioclase crystal margins occasionally have a resorbed texture with 50% amber glass inclusions. A few crystals of amphibole replacing cpx. These crystals, in turn, have rims of fine-grained opaques as well as biotite and cpx. A few of the smaller amphibole crystals have well-defined morphologies, but do have a darker brown, rounded core (cpx?). Also, a trace of well-preserved magmatic pyrite-pyrrhotite present in all crystalline phases (as well as the matrix).

TJ-58; vitrophyre of biotite latite <u>ash</u> flow; 39° 52′ 18" N, 112° 02′ 54" W

Plagioclase, biotite, cpx, titanomagnetite, apatite. Notable difference between this sample and the last one, is the abundance of broken phenocrysts in this sample [which would correlate w/ the occurrence of pumice just above this sample locality - more of an ash-flow origin]. The matrix is definitly more hetrogeneous in terms of orientation of flow foliation. I would classify this as a welded ash flow tuff. Symplectic spinel-cpx crystals, amber glass around glomeroporphyritic clost, perlitic cracks, glass inclusions along plag crystal margins, strongly suggest that this sample is comagmatic w/ the last (TJ-55), However, I didn't find the trace of hornblende overgrowing cpx in this sample.

TJ-59; biotite latite flow; 39° 52′ 30" N, 112° 02′ 54" W

Phenocrysts of plagioclase, clinopyroxene, titanomagnetite, and biotite with apparently abundant phenocrysts of hornblende which may or may not be altered. A few good outlines of amphibole shape are preserved. This is obviously a gas-rich flow. Some coronas of oxides around biotite margins. The matrix is well-crystallized with plag, cpx, oxides, and still a bit of isotropic glass.

TJ-63a; biotite latite flow; 39° 51′ 55" N, 112° 02′ 05" W

Plagioclase, clinopyroxene, biotite, titanomagnetite, and uralitic hornblende after cpx. The plagioclase is often resorbed (except for the rims). The phenocrystes are euhedral and unbroken. The matrix is very fine-grained w/ plagioclase microlites.

TJ-64; biotite latite vitrophyre; 39° 52′ 07" N, 112° 02′ 08" W

Plagioclase, clinopyroxene, biotite, titanomagnetite. A substantial number of broken crystals and moderate variation to the matrix; no pumice lapilli, but substantial oxidation to the glass and deep color to the biotites would suggest that this may be more of an ash-flow vitrophyre. Some areas of the matrix contain distinct amber fragments of glass (or amber glass w/ "bubbles").

TJ-67a; biotite latite flow vitrophyre; 39° 51′ 01" N, 112° 02′ 14" W

Very similar to other latite flow samples (ie TJ-55) Plagioclase, cpx, biotite, titanomagnetite, and hornblende phenocrysts. Plagioclase margins (rather than cores) are resorbed with glass-filled areas. Amber glass in clots and in melt inclusions. The honrblende may be a little

altered (cloudy appearance in cross polars); however, the are a few small crystals of hornblende (similar to TJ-55) that may be primary rather than after cpx and appear unaltered. Even some of the cores of the small hornblende have a distinct appearance similar to those in TJ-55. I would say this is exactly the same flow as TJ-55.

TJ-73; biotite latite flow; 39° 50′ 21" N, 112° 02′ 01" W
Plagioclase, clinopyroxene, (opx?), biotite, titanomagnetite, apatite. Very little oxidation along biotite margins. Cpx distinctly more abundant than biotite.

TJ-75; ryholite of Keystone Springs; (TJ-75; 39° 48′ 22" N, 112° 02′ 56" W)
Sanidine, plagioclase, oxybiotite, oxyhornblendes, titanomagnetite phenocrysts. Some cpx may have been present at the cores of some of the hornblende, but hard to tell.

TJ-77; 39° 48′ 09" N, 112° 03′ 01" W
Plagioclase, sanidine, basaltic hornblende, biotite, Fe-Ti oxides. Difficult to tell if the hornblende originated from cpx. In refelcted light it appears to have a trace of very small pyrrhotite crystals within plagioclase. The titanomagnetite crystals all show trellis exsolution lamellae. The pyrrohotite occurs only in locations which may have been protected from degassing.

TJ-80a; biotite latite flow; 39° 48′ 10" N, 112° 02′ 33" W
Plagioclase, clinopyroxene, opx, hornblende, biotite, oxides and apatite. Very little biotite compared to other flow units. More biotite was present initially, but it has been converted to relict biotite-shaped clots of opx, magnetite, and sanidine. There are also discreet, euhedrel crystals of opx

(esp. smaller ones). Small pyrrhotite/pyrite inclusions in titanomagnetite and pyroxene. All of the inclusions are roughly spherical with a relatively constant ratio of pyrite to pyrrhotite (judging from the different reflectivities) and none larger than ~20 microns.

TJ-80b; mafic flow; 39° 48′ 10" N, 112° 02′ 33" W

Plagioclase, orthopyroxene, clinopyroxene, sanidine, titanomagnetite, ilmenite and hornblende. A few finer-grained clots of sanidine, magnetite, and opx suggest the former presence of biotite since similar clots are cored with biotite in TJ-80a. This suggests an antithetic relationship between the occurrence of biotite and opx-sanidine in these lavas. The matrix consists of plagioclase and magnetite microlites and "glass". Amphibole is also replacing the opx on occasions. No cpx (only opx) is found in the glomeroporphyritic clots. In reflected light, it is apparent that exsolved ilmenite is the dominant (Fe-Ti oxide, w/ (equal or) lesser titanomagnetite which is also exsolved (oxidation). Pyrrohotite is present in moderate sized (15 microns) spheres in pyroxene. However, I have seen several larger spheres which contain a few spongy stringers of hematite, which may represent degassed sulfides. One of these grains is ovoid, has a platey structure and is 150 microns across. One large pyroxene crystal has numerous ovoid cavaties with a platey structure that obvious housed the sulfide phase at one time. One of the spongy hematite holes I found still has a bit of sulfide in it. I think the sulfide inclusions are present in opx and certain zones in the zoned

plagioclase - possibly magma mixing was significant in generating the sulfide phase.

TJ-83; Biotite Latite Intrusion; 39° 50′ 32" N, 112° 03′ 54" W

Seriate textured porphyry consisting of "phenocrysts" of plagioclase, clinopyroxene, titanomagnetite. Biotite was likely present prior to deuteric alteration, but has been replaced by othr phases such as cpx and oxides or the amphibole. Potassium feldspar is undoubtedly present in the matrix, but is not apparent as a phenocryst. Pyrrhotite is also present, but not as abundant as in TJ-84. Many large degasses voids (filled with Fe oxides) represent the former presence of more abundant sulfide blebs.

TJ-84; biotite latite dike; 39° 50′ 33′ N, 112° 03′ 53" W

Plagioclase, clinopyroxene, biotite, hornblende(??), titanomagnetite and an undetermined phase with high interference colors which replaces the cpx phenocrysts, glass in glomeroporphyritic clots. This phase may be fine-grained clays. Titanite replacing cpx in some cases. The matrix in this sample is quite variable and exhibits strong flow foliation. There are many broken crystals and crystal shards which allow the possibility that it fed on ash-flow eruption. Both cpx and plag contain hornblende or biotite inclusions. Lighter and darker zones in the matrix may, in part, reflect a variable abundance of magmatic sulfieds. There are at least three types of sulfide occurrences: 1) rounded blebs as inclusions in all crystalline phases (but particularly titanomagnetite + cpx); 2) wispy aggregates of small grains

parallel to flow foliation in the matrix; 3) platy grains mantling Fe-Mg silicates such as cpx.

TJ-89; biotite latite flow vitrophyre; 39° 50′ 29" N, 112° 03′ 09" W

Phenocrysts of plagioclase, diopside, biotite, and titanomagnetite in a brown glassy matrix with perlitic cracks. Some crystal fragments are present, but not enough welded texture to classify this as an ash-flow vitrophyre. I found a few sulfide grains in the matrix which are angular to platy and about 1-3 microns in size. The titanomagnetite is about 80% converted to hematite or maghemite, but only a few 10 micron grains embedded deep in cpx are totally unaffected. I did find one good circular sulfide bleb ~15 microns in diameter in cpx, but I find the small platy ones (up to 15 microns in length) in the matrix regularly.

TJ-98b; Silver City Monzonite; 39° 50′ 29" N, 112° 03′ 09" W

Phenocrystic phases similar in abundance, size and relative proportions to other monzonite samples. All original Fe-Mg silicates have altered to calcite, chlorite, and a trace (?) of epidote w/ uralitic hornblende (?) around the relict margins of cpx. Much more prominent quartz fills miarolitic cavaties with calcite at the centers.

TJ-92c; Xenolithic inclusion in biotite latite; 39° 48′ 58" N, 112° 01′ 57" W

Most of the opaque phases are be hercynite (80%), followed in abundance by titanomagnetite (~20%) and finally pyrite/pyrrhotite/hematite relicts (trace). The primary sulfide grains are always small (5-10 microns); however, large spongy hematite (degassed sulfide) may be up to 50-100 microns. Exsolu-

tion of titanomagnetite and hercynite are minor or non-existent except along late fractures in the sample. Some different colors + reflectivities in some hercynite grains suggests that some variation in composition is possible. Some fresh sulfide up to 40 microns.

TJ-94; mafic flow; 39° 50′ 50" N, 112° 04′ 47" W

Plagioclase, cpx, opx, titanomagnetite and apatite phenocrysts in an ophitic matrix. However, the matrix glass or pyroxene has been converted mostly to clay and traces of calcite. This type of "alteration" is present in plag phenos which had large melt inclusions. In reflected light, the only apparent Fe-Ti oxide is unexsolved (?) titanomagnetite. Spherical pyrrhotite indusions are rare; when they are present, they are about 50% sulfide + 50% spongy hematlite. Most sulfide occurs as irregular grains in constellations less than 15 microns in size in the matrix. No evidence of relict oxidized biotite.

TJ-95; biotite latite flow; 39° 50′ 03" N, 112° 04′ 07" W

Phenocrysts of plagioclase, cpx, biotite, titanomagnetite and a trace of uralitic hornblende replacing cpx. Phenocrysts are mildly broken w/ crystal shards mildly flow foliated. Sub ophitic matrix.

TJ-96; Sunrise Peak Monzonite intrusion; 39° 50′ 06" N, 112° 04′ 51" W

Phenocrysts of plagioclase, cpx, biotite, titanomagnetite, and moderate-to-weakly developed uralitic hornblende rims on some of the cpx. Texture trends towards seriate, but mostly porphyritic + fine-grained matrix w/ no flow foliation or broken crystals. Abundant calcite in voids and along frac-

tures in cpx.

TJ-97b; Silver City Monzonite intrusion; 39° 51′ 11" N, 112° 03′ 24" W

I am examing the b section first because it is theoretically the least altered of the three. Phenocrysts of plagioclase, clinopyroxene, biotite, and titanomagnetite - cpx has been completely replaced by chlorite, calcite, and a trace of epidote. Only about 10 % of the biotite remains unaltered - the alteration product contains a high proportion of epidote. Quartz is present in the matrix with some of the larger crystals partially filling voids created by alteration of other phenocrysts. In reflected light only about 30% of the titanomagnetite has been altered to hematite. Suprisingly little pyrite (in crystals 10 microns or less) is present in this sample. It must have a few widely scattered large pyrite cubes which I have not seen. I found just a few of the 5 micron spherical inclusions in titanomagnetite and other phenocrysts.

TJ-97a; Silver City Monzonite; 39° 51′ 11" N, 112° 03′ 24" W

Sparse phenocrysts of plag, cpx, biotite, and titenomagnetite which have been largely replaced by chlorite, calcite, minor quartz and oxides, and a mixture of uralitic amphibole and/or epidote. The uralitic amphibote does not have the amphibole shape; and is generally restricted to cpx margins and the matrix. Titanomagnetite is much more worm-eaten and irregular than TJ-97b and about 70% converted to hemetite. A few small scattered pyrite grains in the matrix, but several of the larger (0.2 -0.4 mm) pyrite crystals are also scattered around.

TJ-97c; Silver City Monzonite; 39° 51′ 11" N, 112° 03′ 24" W

Many large euhedral phenocrysts in a fine-grained matrix - not at all seriate, but some variation in matrix crystal size. The brown color of this sample is imported by the wide spread brown epidote which is abundant in every phase. Chlorite often comprises the remainder of the biotite-cpx phases.

Blood red hematite coatings scattered everwhere and much less titanomagnetite than normal with about 95% converted to hematite. Large XIs are even more "badly eaten" and small crystals are almost nonexistent. A lot of anhedral rutite or lecoxene is scattered through altered Fe-Mg silicates and Fe-Ti oxides, but I found no pyrite.

TJ-102; Mafic Flow; 39° 50′ 05" N, 112° 04′ 37" W

TJ-108; Upper Biotite Latite Flow; 39° 49′ 21" N, 112° 04′ 07" W

TJ-112; Sunrise Peak Monzonite Porphyry; 39° 52′ 44" N, 112° 05′ 15" W
Plagioclase, clinopyroxene, biotite, oxides, and relicts of hornblende (?) which are replaced by oxides + chlorite + clay + sericite.

TJ-153; Silver City Monzonite Porphyry; 39° 51′ 37" N, 112° 04′ 20" W

APPENDIX 2: DESCRIPTION OF MAP UNITS

SEDIMENTARY OR EXTRUSIVE UNITS

Qal **Quaternary Alluvium** - Poorly consoloidated deposits of alluvium or talus.

Tlr **Latite Ridge Latite (?)** - White to reddish brown ash flow (and airfall ?) tuff. Outcrops of this unit are typically very altered in all mapped exposures. This phenocryst poor unit (<25% crystals) exhibits small crystals of sanidine and plagioclase and minor relict biotite. Eutaxitic texture apparent in some samples.

Tbu **Biotite latite flows undivided** - Black to gray to reddish brown lava flows and vitrophyres with conspicuous phenocrysts of biotite and plagioclase in hand sample. Clinopyroxene, titanomagnetite, and apatite are always apparent in thin section, but orthopyroxene, amphibole, sanidine and magmatic sulfide blebs may or may not be present.

Tblu **Upper biotite latite flows** - Black to gray lava flows and vitrophyres with prominent biotite and plagioclase in hand sample. Clinopyroxene, orthopyroxene, titanomagnetite, apatite, and magmatic sulfide blebs are also present, but not obvious in hand sample. Distinguished from other biotite latite flow sequences, in the field, only on the basis of stratigraphic position - these are stratigraphically above the mafic flow sequence.

Tmf **Mafic flows of Buckhorn Mountain** - Dark to variably colored flows, breccias, and agglomerates with little or no apparent biotite in hand sample. These flows and breccias are often vesicular (often with very elongate vesicles) and mildly altered. Clinopyroxene, plagioclase, orthopyroxene, titanomagnetite, rare olivine, apatite, traces of magmatic sulfides and a few strongly resorbed and oxidized relict biotite crystals can also be found.

Tblf **Lower biotite latite flows** - Light gray to red brown lava flows with conspicuous biotite and plagioclase in hand sample. Clinopyroxene, titanomagnetite, apatite, and on occasion amphibole and magmatic sulfide blebs (?) can also be found in these flows. Distinguished

from other biotite latite flow units in the field based on a stratigraphic position beneath the mafic flow unit.

Tse **Epiclastic sediments** - Poorly stratified volcaniclastic sediments and conglomerates. Original composition often obscurred by intense alteration. Intense alteration may have been facilitated by an originally high pumice or carbonate content (apparent in a few outcrops). Rarely, angular clasts of Tintic Quartzite or other Paleozoic carbonate units are present.

Tsu **Upper lacustrine sediments** - Mudstone and shale with carbonaceous remains of plant material and fresh water limestone. Generally very poorly exposed. Multiple thin horizons of this lithology may be present around Buckhorn Mountain intercalated with the biotite latite flows.

Tspf **Flows and agglomerates of Sunrise Peak** - Light green to light brown slabby-weathering flows in which plagioclase crystals are conspicuous in hand sample. Other phenocrystic phases include biotite, clinopyroxene, titanomagnetite, and apatite. Field relations and composition suggest that the flows vented from the Sunrise Peak Stock (and associated dikes). The agglomerate occupies the same stratigraphic position and contains the same phases except that biotite is larger in size and more abundant in both fresh and altered outcrops.

Tsl **Lower lacustrine sediments** - Light colored fissile shale, siltstone, and volcaniclastic sandstone. Exhibits ovoidal structures replaced by pyrite which may represent gastropods.

Tct **Tuff member of Copperopolis Latite** - Phenocryst-poor ash flow tuff which is everywhere intensesly altered. Suspected relict phenocrysts of plagioclase and biotite.

INTRUSIVE UNITS

Tks **Rhyolite of Keystone Springs** - Near-surface domes or intrusive plugs of light-colored feldspar porphyry. Conspicuous large crystals of sanidine and plagioclase with much smaller minor crystals of biotite, titanomagnetite, amphibole and traces of magmatic pyrrhotite.

Tsc **Silver City Monzonite Porphyry** - Phenocryst-rich, amphibole-bearing monzonite porphyry with a seriate texture. Some variation in size, abundance, and relative proportions phenocrysts is often present within the same dike or plug. Quartz and amphibole are present in the more "phenocryst-rich" lithologies. Clinopyroxene, biotite, plagioclase, and magnetite are early-formed phases; orthoclase, apatite, sphene, and zircon are also present. Hydrothermal alteration expressed as epidote, chlorite, and minor clay, sericite, and pyrite is almost ubiqutous.

Tli **Biotite latite intrusions** - Dark-colored vent-facies dikes and plugs, occasionally exhibiting columnar jointing inward from the walls of the dike. Compositionally identical to the biotite latite flows.

Tsp **Sunrise Peak Monzonite Porphyry** - Distinctly porphyritic monzonite with a consistently fine-grained groudmass and fewer phenocrysts than Silver City Monzonite Porphyry. Conspicuous pheoncrysts include plagioclase, clinopyroxene, biotite, and magnetite.

HYDROTHERMAL ALTERATION

Ta **Argillic-phyllic alteration** - The dominant minerals of this alteration are clay, sericite, and pyrite (generally oxidized to limonite).

Ts **Silicification** - Rpresented by substantial additions of silica to the rock to produce chert, jasperoid, or strongly silicified wallrocks around a vein or fracture.

PLATE I

GEOLOGIC MAP OF TERTIARY ROCKS IN THE CENTRAL EAST TINTIC MOUNTAINS, UTAH

CORRELATION OF UNITS

SEDIMENTARY AND EXTRUSIVE	INTRUSIVE	
Qal		
Tlr	Tbu, Tblu, Tmf, Tblf	Tks, Tsc, Tli
Tse, Tsu		
Tspf	Tsp	
Tsl		
Tct		

Eocene - Oligocene

Geology by J.D. Keith and C.S. Kim (1985-88).

EUREKA QUADRANGLE
UTAH
7.5 MINUTE SERIES (TOPOGRAPHIC)

TINTIC MOUNTAIN QUADRANGLE
UTAH
7.5 MINUTE SERIES (TOPOGRAPHIC)

Mapped, edited, and published by the Geological Survey

Control by USGS and NOS/NOAA

Topography from aerial photographs by multiplex methods
Aerial photographs taken 1950. Field check 1954

Polyconic projection. 1927 North American datum
10,000-foot grid based on Utah coordinate system, central zone
1000-meter Universal Transverse Mercator grid ticks,
zone 12, shown in blue

Dashed land lines indicate approximate locations

Unchecked elevations shown in brown

Revisions shown in purple compiled from aerial photographs taken 1975. This information not field checked

UTM GRID AND 1975 MAGNETIC NORTH DECLINATION AT CENTER OF SHEET

SCALE 1:24 000

CONTOUR INTERVAL 40 FEET
NATIONAL GEODETIC VERTICAL DATUM OF 1929

THIS MAP COMPLIES WITH NATIONAL MAP ACCURACY STANDARDS
FOR SALE BY U. S. GEOLOGICAL SURVEY, DENVER, COLORADO 80225, OR RESTON, VIRGINIA 22092
A FOLDER DESCRIBING TOPOGRAPHIC MAPS AND SYMBOLS IS AVAILABLE ON REQUEST

ROAD CLASSIFICATION

Primary highway, hard surface
Secondary highway, hard surface
Light-duty road, hard or improved surface
Unimproved road
Interstate Route
U. S. Route
State Route

QUADRANGLE LOCATION

EUREKA, UTAH
N3952.5—W11200/7.5

1954
PHOTOREVISED 1975
AMS 3563 I NE—SERIES V897

TINTIC MOUNTAIN, UTAH
N3945—W11200/7.5

1954
PHOTOREVISED 1975
AMS 3536 I SE—SERIES V897

INTERIOR—GEOLOGICAL SURVEY, RESTON, VIRGINIA—1978

AND HYDROTHERMAL ALTERATION

PLATE 2